

Spectroscopic Insights in the Metalation and Dehydrogenation of Tetrapyrroles on Well- Defined Metal Substrates

Spektroskopische Einblicke in die Metallierung und Dehydrogenierung von Tetrapyrrolen auf wohldefinierten Metallsubstraten

Der Naturwissenschaftlichen Fakultät der
Friedrich-Alexander-Universität Erlangen-Nürnberg

zur Erlangung des Doktorgrades Dr. rer. nat.

vorgelegt von
Michael Dominic Röckert
aus Nürnberg

Als Dissertation genehmigt

von der Naturwissenschaftliche Fakultät

der Friedrich-Alexander-Universität Erlangen-Nürnberg

Tag der mündlichen Prüfung: 18.05.2015

Vorsitzender des Promotionsorgans: Prof. Dr. Jörn Wilms

Gutachter: Prof. Dr. Hans-Peter Steinrück

Prof. Dr. Jörg Libuda

Contents

1. Introduction	1
2. Preliminary Work	3
2.1 Adsorption Behavior of Tetrapyrroles on Metal Surfaces.....	3
2.2 Metalation of Tetrapyrroles on Metal Surfaces.....	4
3. Experimental Methods	7
3.1 X-ray Photoelectron Spectroscopy (XPS)	7
3.1.1 The Photoemission Process	7
3.1.2 Composition of an XP-Spectrum	8
3.1.3 Coverage Determination with XPS	10
3.2 Temperature-Programmed Desorption (TPD).....	12
3.2.1 Principle of TPD.....	13
3.2.2 Analysis Methods for TPD Spectra.....	14
3.2.3 Optimization of the TPD Setup.....	15
3.3 Ultra-High Vacuum Apparatus and Sample Preparation	17
4. Results	12
4.1 Tetrapyrroles on Cu(111)	20
4.1.1. Coverage- and Temperature-Dependent Metalation and Dehydrogenation of 2HTPP on Cu(111).....	20
4.1.2 Insights into the Self-Metalation Pathway of 2DTTP on Cu(111)	27
4.1.3 Metalation and Conformational Change of 2HTTBPP on Cu(111)	27
4.1.4 Metalation and Layer Exchange Mechanism of 2HPc on Cu(111).....	30
4.2 Metalation of Tetraphenylporphyrin with Iron on Ag(100)	31
5. Summary and Outlook	33
6. Zusammenfassung und Ausblick	35
7. Acknowledgement	38
8. List of Figures	40
9. List of References	42
10. Appendix [P1] – [P6]	49

1. Introduction

'Physicists and chemists perceive one similarity within the rain of Ireland, the Red Sea, the Titicaca Lake and the dew in my garden: It is always H₂O!'

(Michel Tournier, french writer) [1]

Beyond the literary merit of this phrase, I want to draw the reader's attention to the common building block, namely water. We already know the physical and chemical properties of water on a fundamental level [2-4] and can therefore easily explain the different appearances; a single drop (rain), homogenous fluid (sea) or the liquid film that covers the surface of a leaf (dew). Hence, once properties are understood on a fundamental level that knowledge can be applied to many, seemingly very different, systems and used to get new insights in those systems.

One prominent group of organic building blocks that, just as water, is important in our daily life is the tetrapyrroles. The reason for their importance can be found in the molecular structure, which consists of four pyrrole-like rings linked by methine bridges (depicted in Figure 1).

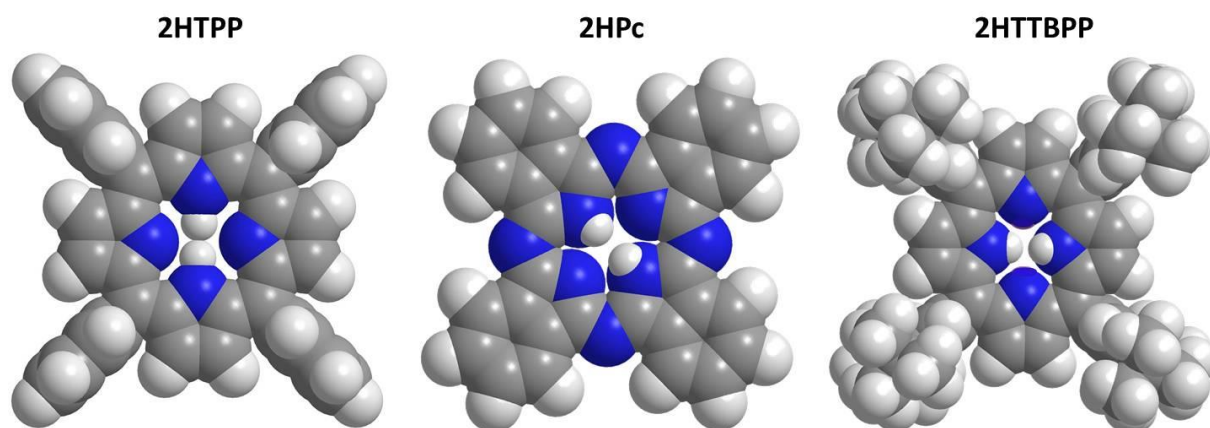


Figure 1: Space filling models of 2H-tetraphenylporphyrin (2HTPP), 2H-phthalocyanine (2HPc) and 2H-tetrakis-(3,5-di-tert-butyl)-phenylporphyrin (2HTTBPP).

1. Introduction

The resulting carbon framework has a delocalized π -electron system and obeys Hückel's rule of aromaticity [5-7]. One well-known member of the tetrapyrroles is the porphyrin, the main focus of this thesis. For biological processes, mostly metalloporphyrins are relevant, i.e. porphyrins that have a metal atom coordinated in the central cavity. A prominent example is the Fe-porphyrin derivative in hemoglobin [8, 9], where the central iron atom is able to bind oxygen and is, thus, responsible for oxygen transport in mammals. However, carbon monoxide (CO) also binds to the metal center of the iron porphyrin, and, because CO has a higher affinity to the iron center than oxygen, oxygen is competitively replaced, and we can, thus, explain why the inhalation of carbon monoxide leads to asphyxiation [10-14]. The knowledge of the reactivity of the central metal atom towards small molecules has already successfully been used for biomimetic catalysts, e.g. to the reduction of oxygen with either Fe-porphyrin like carbon nanotubes [15] or Pt-porphyrins [16] or to sensor applications [17, 18].

Due to their large delocalized π -electron system, tetrapyrroles have intense light absorption bands in the visible region, which cause their bright colors. This characteristic is also the origin of the name porphyrin, from the Greek word *porphyros*, meaning purple. By attaching suitable ligands, the light absorption properties can be modified. Prominent examples in nature are Cu-porphyrins, which cause the brown-red color of the flight feathers of the tropical bird family *Musophagidae* [19] and the green Mg-porphyrin derivative, responsible for light absorption in chlorophyll [20, 21]. Porphyrins can also be found as photon converters in solar cells [22-25] and active substance in medical photodynamic therapy [26, 27].

However, we have not yet arrived at a complete fundamental understanding of these molecules. The present study concentrates on two fundamental reactions not yet fully understood, namely the metalation and the dehydrogenation of tetrapyrroles on metal surfaces. The investigated systems include three tetrapyrrole molecules, namely 2H-tetraphenylporphyrin (2HTPP), 2H-phthalocyanine (2HPc) and 2H-tetrakis-(3,5-di-tert-butyl)-phenylporphyrin (2HTTBPP), on Cu(111) and Ag(100). The main investigative methods used were X-ray photoelectron spectroscopy, to study the adsorbed reactants and reaction products, and mass spectrometry, to study the volatile reaction products.

2. Preliminary Work

2.1 Adsorption Behavior of Tetrapyrroles on Metal Surfaces

The interaction of large organic molecules, such as tetrapyrroles, with metal surfaces is typically dominated by van der Waals interactions. In order to maximize the van der Waals interactions, the molecules, therefore, usually adsorb with the macrocycle parallel to the surface [28]. The adsorbed molecules are also often slightly deformed compared to the gas phase conformation, with inert side groups, such as phenyl and tert-butyl, rotated and/or bent away from the surface while more reactive groups, such as imine (-N=), bent down towards the surface [29-55]. The lateral ordering of the molecules is usually determined by a competition between molecule-substrate interactions and molecule-molecule interactions [29-55]. For 2HTPP on Ag(111) and Au(111), the molecule-substrate interaction is weak and T-type interactions between the phenyl groups of neighboring molecules dominate, producing a well-ordered, long-range square lattice [37, 56-58].

Due to coadsorption of small molecules, such as NO, the long-range order of porphyrins can be modified. Buchner *et al.* reported that Co-tetraphenylporphyrin (CoTPP) on Ag(111) is arranged in a quadratic lattice at room temperature, with a unit cell of 1.91 nm². Upon high NO exposure (at room temperature), CoTPP reorganizes and a number of well-ordered intermixed NO+CoTPP phases are formed, while the size of the unit cell is increased up to 3.16 nm². This behavior can be interpreted as due to attractive lateral dipole-dipole interactions between the two species [57].

For 2HTPP on Cu(111), the molecule-substrate interaction is stronger and the imine groups bend down towards the surface deforming the molecule [31, 32, 34, 38, 39, 50, 52, 54, 59]. The stronger molecule-substrate interaction also pulls the molecule down towards the surface, forcing the phenyl rings to tilt further and become almost parallel to the surface, preventing the T-type interactions between phenyl rings of neighboring molecules [38]. The combination of the stronger localized covalent bond between the iminic nitrogen atoms and the surface and the weaker T-type interactions means that, at low coverage, 2HTPP adsorbs on Cu(111) as individual molecules aligned along the substrate rows, but without any long range ordering. At coverages above 0.37 molecules/nm², an ordered checkerboard structure begins to form

2. Preliminary Work

with every second molecule elevated slightly above the surface, allowing stabilizing T-type interactions between the elevated molecules and the lower molecules [34]. As 2HTPP metalates on Cu(111) to CuTPP, the interaction between the iminic nitrogen atoms and the surface is lifted, pushing the molecule away from the surface, allowing the phenyl rings to rotate and form T-type interactions between neighboring molecules. As a consequence, CuTPP forms ordered square islands on Cu(111), but the weak interaction also makes the molecules highly mobile on the surface, and the islands will coexist with a 2D gas phase that is too mobile to be imaged at room temperature with STM [32, 38, 52].

It is, furthermore, possible to form extended networks by forming covalent bonds between molecules, such as the C-Cu-C coupling of neighboring porphyrins on Cu(110) or Au(111) [60, 61].

2.2 Metalation of Tetrapyrroles on Metal Surfaces

Tetrapyrroles exist as free-base molecules, as depicted in Fig. 1, or as metalated molecules, where the two central aminic protons have been replaced by a central metal atom. Many metallotetrapyrroles can be deposited directly on surfaces, but, some reactive metalloporphyrins, such as FeTPP often require stabilizing ligands in air. By instead metalating the porphyrins *in situ*, on the surface, such ligands can be avoided [42].



The metal atoms can either be co-deposited on the surface together with the tetrapyrrole molecules or in the case of metal substrates be extracted directly from the surface; the latter is also called self-metalation [50-52, 62, 63]. XPS and STM measurements have demonstrated metalation with cobalt, iron, zinc, copper, nickel and cerium [30, 31, 33, 36, 41-52, 62, 63]. Utilizing an STM tip, even metalation with Ag was possible [64]. Metalation is easily followed by XPS, as depicted in Figure 2 for the self-metalation of 2HTPP on Cu(111).

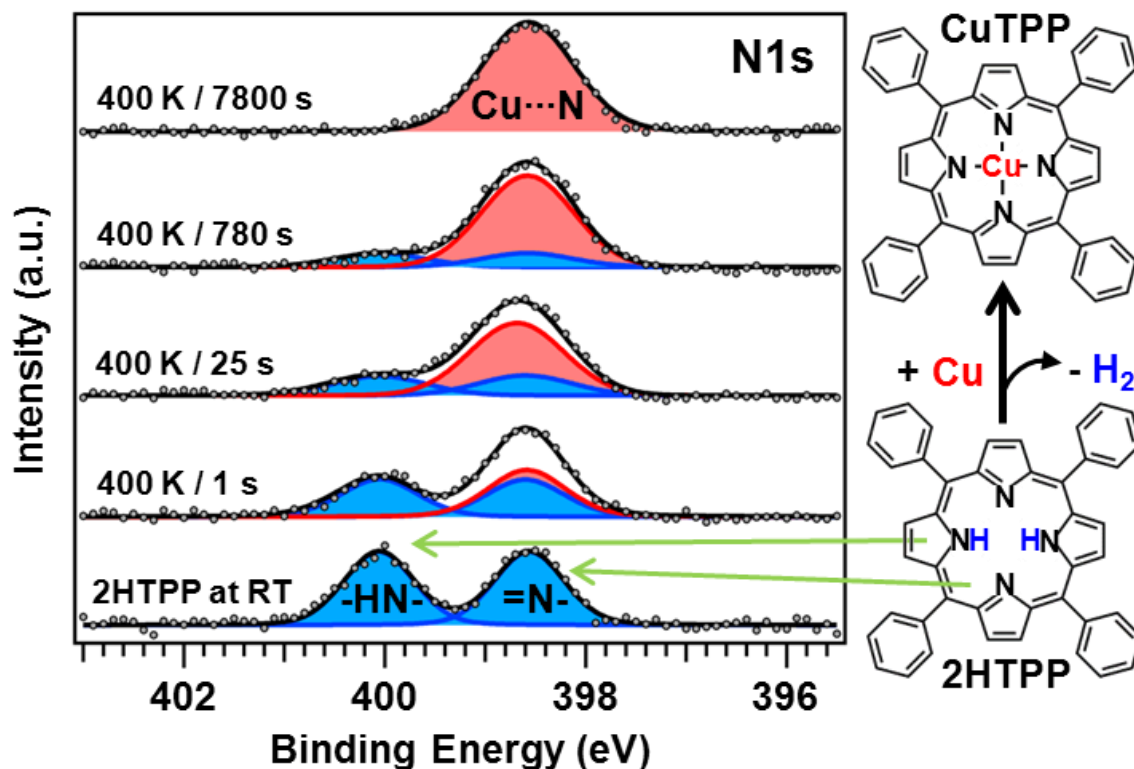


Figure 2: As $0.41 \text{ molecules/nm}^2$ 2HTPP metalate on Cu(111), the two N 1s photoemission peaks, corresponding to the two nitrogen species of 2HTPP, aminic ($=N-$) at 398.55 eV and the iminic ($-NH-$) at 400.05 eV , merge into the single peak of CuTPP, where all four nitrogen atoms are equivalent.

Free-base tetraphenylporphyrin (2HTPP) contains four nitrogen atoms, two aminic ($-NH-$) and two iminic ($=N-$) nitrogen atoms, easily distinguished in XPS, because of the different local chemical environments, see Figure 2. Upon metalation, the two N 1s photoemission peaks of 2HTPP merge into the single peak of CuTPP ($\text{Cu}\cdots\text{N}$), where all the four nitrogen atoms are bound equally to the central metal atom and are therefore chemically equivalent.

What little is known about the reaction pathway of the metalation reaction has been provided by Density Functional Theory (DFT) calculations by Shubina *et al.* of metalation in the gas phase, which is exemplarily depicted in Figure 3 for the metalation of 2HP with Co [48, 59, 65]. For the gas phase metalation pathway of 2HTPP with Fe, Co, Ni, Cu and Zn it is reported that first the metal atom coordinates to all four nitrogen atoms, while the aminic nitrogen atoms retain their bonding to the hydrogen atoms.

2. Preliminary Work

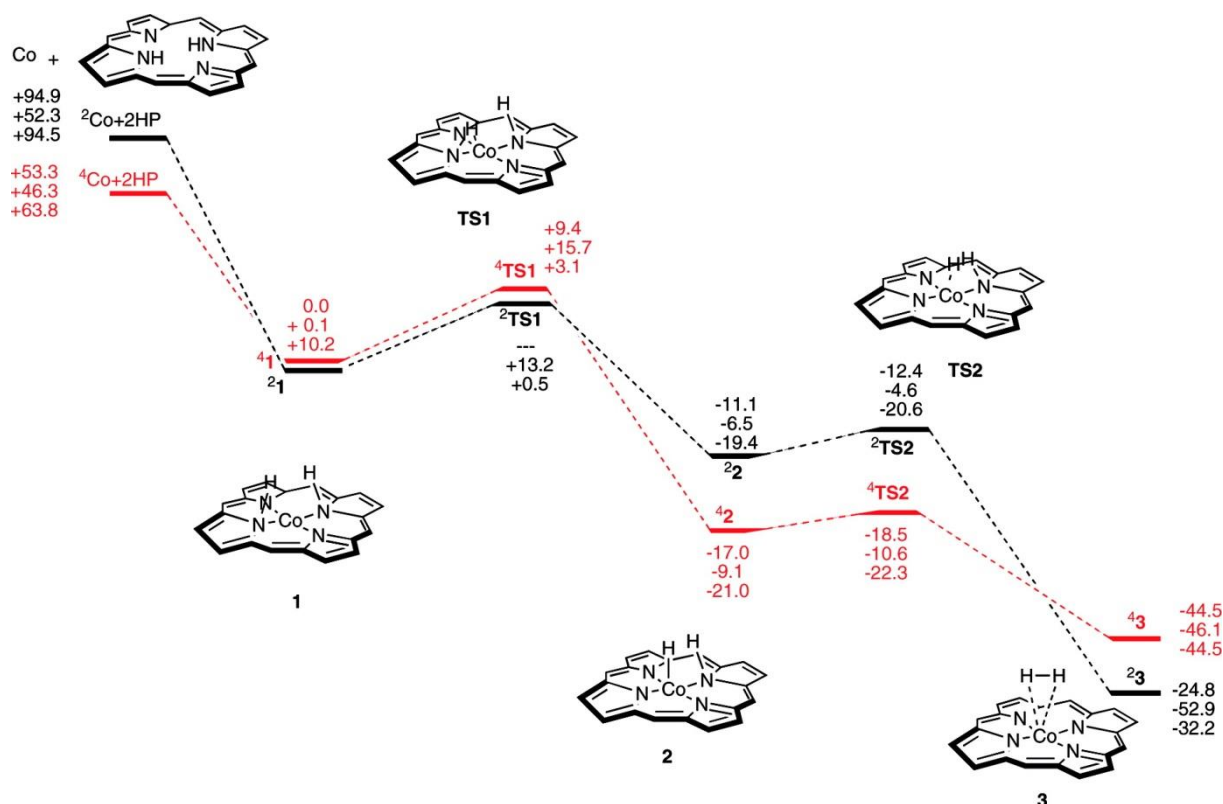


Figure 3: Scheme of the energy profile of the gas phase metalation of 2HP with Co [48].

Subsequently, a two-step reaction happens, where the two aminic hydrogen atoms are consecutively transferred onto the metal center, recombine there and desorb as H₂. The largest energy barrier was found for the transfer of the first hydrogen atom onto the metal center [48]. The last chapter of this thesis will address the first intermediate in the case of metalation of 2HTPP with Fe.

3. Experimental Methods

In this chapter, the theoretical background of X-ray photoelectron spectroscopy (XPS) and temperature-programmed desorption (TPD), also known as thermal desorption spectroscopy (TDS), will be introduced. Afterwards, the ultra-high vacuum apparatus and sample preparation will be presented.

3.1 X-ray Photoelectron Spectroscopy (XPS)

The subsequent chapter is dedicated to give a more detailed description of XPS, a surface sensitive characterization method.

3.1.1 Photoemission Process

XPS is a well-established surface investigation method, based on the photoelectric effect [66]. Upon irradiating a surface with X-ray photons, photoelectrons are emitted and collected with an electron energy analyzer. Knowing the photon energy $h \cdot \nu$, the measured kinetic energy of the excited electron in the analyzer, and the analyzer work function (Φ_s), the initial binding energy (E_B) of the electron can be calculated as follows:

$$E_B = h \cdot \nu - E_{kin} - \Phi_s.$$

Since the energies of the deeper lying atomic orbitals are distinct for each element, the binding energies calculated can be used to identify and quantify the elements present on the surface. Changes in the local chemical environment affecting the electron density (e.g. a change in oxidation state) will, furthermore, shift the atomic orbitals slightly up or down in energy because of simple electrostatic interactions. These “chemical shifts” are usually in the range of few electron volts.

The surface sensitivity of XPS is determined by the inelastic mean free path (λ) of the emitted photoelectron, which is the average distance the photoelectron will travel through matter without losing energy. It is a function of the kinetic energy of the photoelectron and is described by the “Universal Curve” [67], depicted in Figure 4. Limiting the kinetic energy

3. Experimental Methods

range of the photoelectrons to 50-1500 eV, as done by all experiments within this thesis, gives a mean free path of less than five nanometers and therefore a high surface sensitivity.

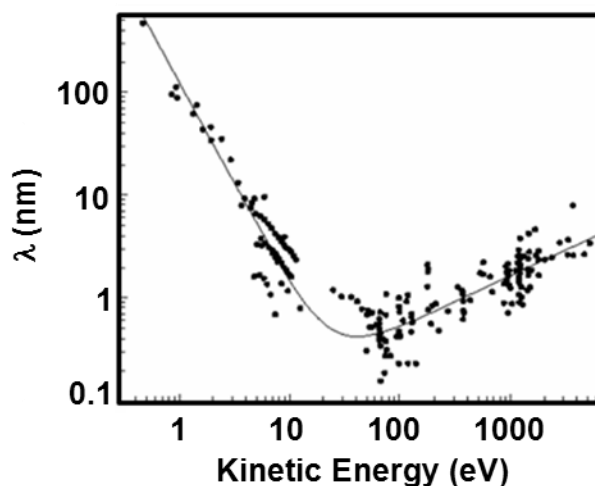


Figure 4: The “Universal Curve”, showing the inelastic mean free path as function of the kinetic energy of electrons [67].

3.1.2 Composition of an XP-Spectrum

An XPS spectrum of a clean Cu(111) surface is depicted in Figure 5. The XP features, caused by photoelectrons, are typically the most intense and most narrow lines (main lines) on top of a broad background. The background is caused by primary photoelectrons that have been inelastically scattered and lost energy. They have sufficient energy to leave the sample, but contribute due to their energy loss to the background at the higher binding energy side of the main line.

From Figure 5, we observe two Cu 2p photoemission peaks ($2p_{1/2}$ and $2p_{3/2}$). This is known as spin-orbit splitting, yielding to two states, with a total angular momentum (j) of each state $j = 1/2$ and $j = 3/2$, respectively. The intensity ratios are based on the degeneracy of each state, i.e. the number of all possible combinations to generate the total j value ($2j + 1$). This results in an intensity ratio of 2:4 for Cu $2p_{1/2}$: Cu $2p_{3/2}$.

When an atom already has an unpaired electron before the core hole is created, very complicated peak structures, known as multiplett splitting, may occur. The actual mechanism is quite complicated and is still under scientific discussion [68-71]. To put it simply, the

3. Experimental Methods

coupling mechanism can be explained as follows: after creating a core hole, the unpaired electron in the core level can couple with the unpaired electron in the outer shell, giving rise to several energetically different final states, which then lead to complex peak patterns.

The XP spectrum in Figure 5 also has three very broad peaks (Cu LMM, LMV and LVV). These are Auger peaks. After the photoelectron has left the sample, the vacancy can be filled by a second electron from a higher energy level, releasing energy either as a photon (X-ray fluorescence) or a third electron which leaves the atom (Auger decay). The kinetic energy of the Auger electron is, thereby, independent of the photon energy used to create the core hole and depends only on the energy levels of the three electrons involved. For inner core holes of heavier elements X-ray fluorescence dominates, whereas for lighter elements and outer orbitals of the heavier elements the Auger process dominates.

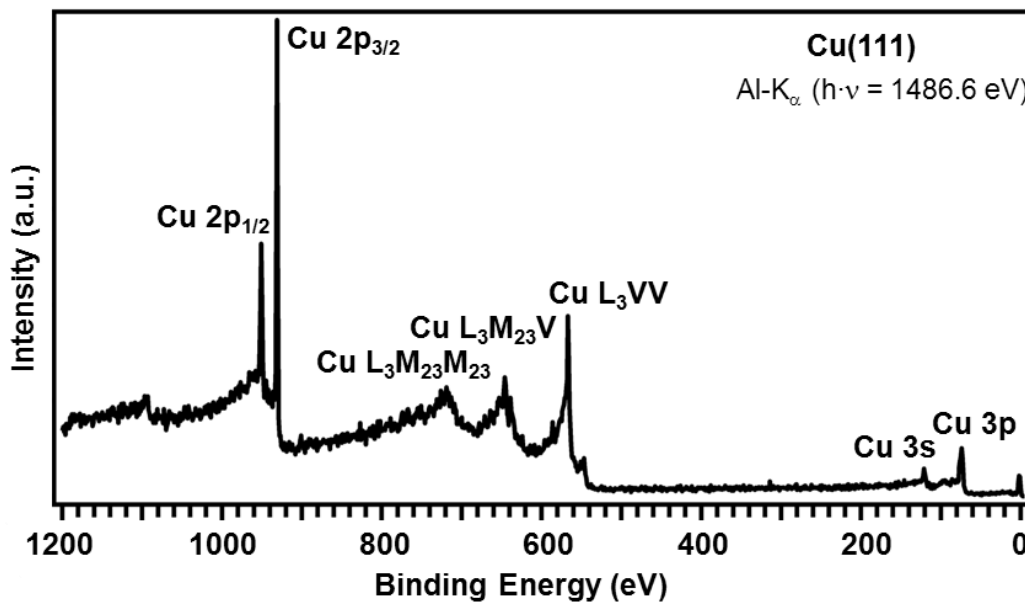


Figure 5: XPS spectrum of a clean Cu(111) surface, within the respective XP features are labeled.

Besides the aforementioned features, a photoelectron spectrum may contain partial intensities from other processes. As not all processes are relevant for the current thesis, the interested reader is referred to the textbook of Hüfner [72] and Oura et al. [73].

To identify or quantify different chemical states, which are very close in energy and therefore not properly resolved, overlapping features must be deconvoluted, which is done by fitting multiple peak functions to the data. The measured shape and width of a XPS peak, is a convolution of several contributions, such as: the shape and line width of the excitation

3. Experimental Methods

source, the line shape and width of the photoemission process and the resolution of the analyzers [72]. The line shape of the Al-K $_{\alpha}$ emission line can be approximated by a Lorentzian function, having a line width ΔE_{X-ray} of 0.85 eV before and 0.20 eV after the monochromatization. The intrinsic line shape of the photoemission process can also be described by a Lorentzian curve. The width of the signal ΔE_{NLW} is inversely proportional to the lifetime τ of the core hole and can therefore be estimated by the uncertainty principle [110] as follows: $\Delta E_{NLW} = h/\tau$. For a lifetime $\tau = 10^{-15}$ s, the intrinsic line width of the photoemission process becomes 0.7 eV. The lifetime, generally, decreases with increasing binding energy. The detection of the photoelectrons in the analyzer results in a distinct perturbation of the photoelectrons and can be described by a convolution of the initial Lorentzian with a Gaussian function. The Gaussian broadening is thereby given by the resolution of the analyzer ($\Delta E_A = 0.1$ eV). Thus, the line shape of a XP peak is well represented by a convolution of a Lorentzian and a Gaussian function (Voigt profile) [72, 109]. As the convolution is computational costly, often the simple linear combination of these two functions is applied (pseudo-Voigt) [109, 111]. This procedure is more applicable as it numerical less costly. The normalized pseudo-Voigt function can be described as follows [109]:

$$f_{pV}(x) = (1 - \eta)f_G(x; y_G) + \eta f_L(x; y_L)$$

With $f_G(x; y_G)$ and $f_L(x; y_L)$ the normalized Gaussian and Lorentzian function and η a weighting factor with possible values between 0 and 1.

3.1.3 Coverage Determination with XPS

Besides qualitative information (Chapter 3.1.1-3.1.2) also the quantity of the respective elements can be determined by XPS. However, in a typically experiment where a substrate B is covered by a film of A, see Figure 6, the attenuation of photoelectrons from B travelling through A has to be considered.

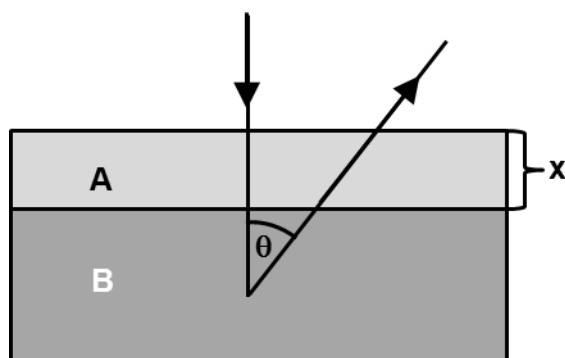


Figure 6: Schematic illustration of a homogenous grown film A with a thickness x on a substrate B.

The number of electrons that after having travelled a length d reach the surface without having lost energy are attenuated according to Lambert Beers` law:

$$I = I_0 \exp\left(-\frac{d}{\lambda}\right)$$

I is the intensity at the surface, I_0 is the intensity at the depth d and λ is the inelastic mean free path. Electrons, which travel along trajectories at an angle to the surface normal, have to travel a distance that equals $d = \frac{x}{\cos\theta}$, where x is the thickness of layer A.

$$I = I_0 \exp\left(-\frac{x}{\lambda \cos\theta}\right)$$

The absolute intensity of photoelectrons originating from a homogenous grown film A on a substrate B, as it can be found by a layer-by-layer growth mode, can be calculated as follows:

$$I_A = I_{A\infty} \left[1 - \exp\left(-\frac{x}{\lambda_A \cos\theta}\right)\right]$$

The intensity I_A is a measured value and corresponds to the quantity of a specific element, which is only present in the film A, such as the C 1s intensity of an organic film grown on a metal substrate. $I_{A\infty}$ is the intensity of the pure bulk matter of A, i.e. the intensity value if the film thickness of A increases to infinity. This value can be experimentally measured by increasing the coverage of A till the count rate saturates at its maximum value. For the attenuation of the substrate intensity by covering the surface with and film A, the layer thickness can be estimated as follows:

3. Experimental Methods

$$I_B = I_{B\infty} \exp\left(-\frac{x}{\lambda_B \cos\theta}\right)$$

Calculating the coverage from absolute intensities involves a risk, as changing the sample position (distance to analyzer, emission angle) or a change in the photon flux affects the absolute intensities. To minimize these errors, it is usual to use intensity ratios, as the ratios will not change if the position or photon flux changes. For a layer of A on B, as in Figure 6, the intensity ratio can be written as:

$$\frac{I_A}{I_B} = \frac{I_{A\infty} \left[1 - \exp\left(-\frac{x}{\lambda_A \cos\theta}\right)\right]}{I_{B\infty} \exp\left(-\frac{x}{\lambda_B \cos\theta}\right)} \approx \frac{\sigma^A \left[1 - \exp\left(-\frac{x}{\lambda_A \cos\theta}\right)\right]}{\sigma^B \exp\left(-\frac{x}{\lambda_B \cos\theta}\right)}$$

The resulting equation is a good approximation to calculate the relative coverage of an adsorbate film. The atomic sensitivity factor σ of different elements are based on empirical data sets and can be derived from literature, e.g. from Wagner *et al.* [74]. If the literature value of the sensitivity factors is applied to estimate the quantity of elements, the experimental settings as reported in literature should be applied.

For thin layers and photoelectrons with high kinetic energy, attenuation becomes negligible and the coverage becomes proportional to the ratio $\frac{I_A}{I_B}$. Hence, if a known coverage can be created and measured, the proportionality constant can be determined and used to calculate any unknown coverage. When multilayers of 2HTPP are deposited on Cu(111) and heated above 550 K, the molecules in the multilayers desorb, but 0.46 molecules/nm² remain on the surface, independent of the initial coverage, even upon heating to 1000 K. The exact number of molecules remaining on the surface was determined by Michael Stark and Dr. Stefanie Ditze in the group of PD Dr. Hubertus Marbach by counting the remaining molecules in STM images after heating to 550 K at 2 K/s for 2 minutes and immediately cooling back down to room temperature afterwards.

3.2 Temperature-Programmed Desorption (TPD)

Metalation of tetrapyrroles has a very clear signature in XPS, see Figure 2, but one high quality N 1s spectrum can take up to four hours, especially for low coverages. Recording a

3. Experimental Methods

heating series would, therefore, be extremely slow and the risk of beam damage, i.e. photon induced reactions, very high. For 2HTPP on Cu(111), we observed beam damage already after 6 hours. Dehydrogenation is very difficult to see in XPS, as only small shifts in the C 1s spectrum are expected and hydrogen itself cannot be detected, due to its small cross section [75, 76]. This leads us to temperature-programmed desorption (TPD). Recording one TPD spectrum is typically fast (10 minutes) and it is a very suitable technique to investigate the evolution of hydrogen both during metalation and dehydrogenation.

3.2.1 Principle of TPD

TPD is a surface science technique used to follow reactions that produce desorbing molecules. The principle is rather simple. As the temperature is increased high enough to overcome the activation energy barrier of the given reaction involving desorption, the desorbing products, and thereby the reaction rate, can be detected with a mass spectrometer [77]. Figure 7 shows the hydrogen evolution from the metalation and dehydrogenation of 0.72 2HTPP molecules/nm² on Cu(111).

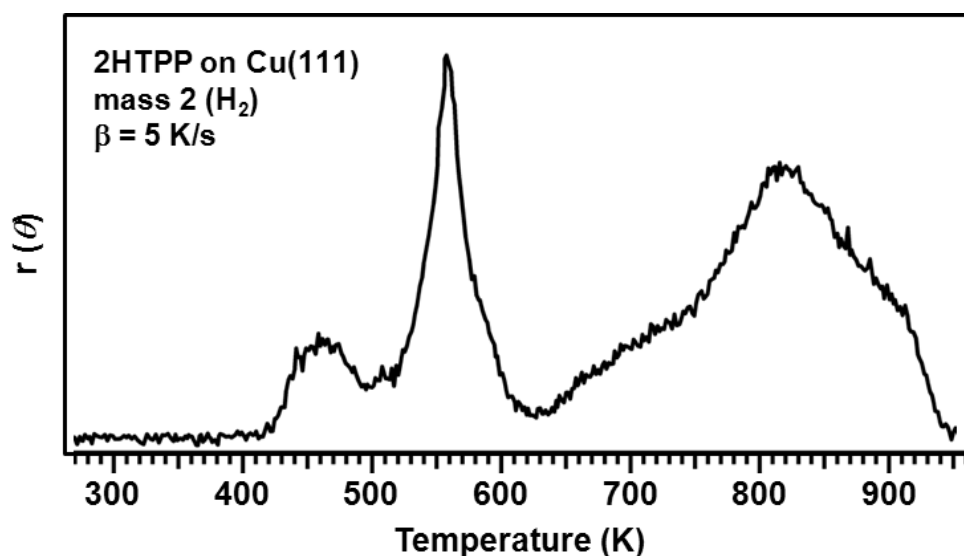


Figure 7: Hydrogen evolution from 0.72 2HTPP molecules/nm² on Cu(111).

If the residence time of the molecules in the mass spectrometer is low enough (that is at high pumping speed), the measured intensity is directly proportional to the reaction rate, which is described by the differential equation by Polanyi-Wigner. Assuming that metalation and dehydrogenation are both first order reactions, the equation becomes:

3. Experimental Methods

$$r(\theta) = \frac{-d\theta}{dt} = v_d \theta_{2HTPP} \exp\left(\frac{-E_a}{RT}\right)$$

with r the reaction rate, v_d the pre-factor, θ_{2HTPP} the coverage of 2HTPP, and E_a the activation energy for the reaction, R the gas constant, T the sample temperature.

3.2.2 Analysis Methods for TPD Spectra

TPD is a good way to get information about reaction temperatures and how many and which molecules desorb during a reaction. However, to get more detailed information of the reaction kinetics, e.g. the activation energy and the pre-factor, analysis methods based on the Polanyi-Wigner equation have to be used [78-85].

The method according to Habenschaden-Kippers, better known as **leading edge** analysis, considers that the pre-factor v_d and the activation energy may both depend on coverage [79]. To keep both parameters constant, a small temperature window at the high coverage side of the TPD spectrum is analyzed, i.e. the leading edge of the spectrum, where the desorption rate and thereby the change in coverage is minimal. The resulting Arrhenius plot gives a straight line with slope $-\frac{E_a}{R}$ and intercept $\ln(\theta) + \ln(v)$. The disadvantage is that the method requires a good signal-to-noise ratio, as a small temperature range is used with a low desorption rate yielding to a reduced accuracy.

By far the simplest approach is the analysis according to **Redhead** [85]. This method is popular, as one needs only the temperature at the desorption maximum T_{max} , which is usually an easy accessible feature. The relation between T_{max} and the desorption energy E_a is given by the differentiation of the Polanyi-Wigner equation, assuming that the pre-factor v and the activation energy E_a are independent of coverage:

$$E_a = -RT \ln\left(\frac{\beta E_a}{vRT_{max}}\right)$$

To find the activation energy, it is necessary to guess a value for the activation energy and then iterate a few times to find an accurate value. However, this method is only valid for first order reactions and linear heating rates β , and one has to predict the pre-factor for desorption. The latter value has to be derived from literature or otherwise is typically set to be 10^{13} s^{-1} .

3. Experimental Methods

However, for reactions or desorption of large organic molecules the pre-factor may be drastically different from 10^{13} s^{-1} [86-91]. For further details the interested reader is referred to the article by de Jong *et al.* [81] and the review by Falconer *et al.* [83] who made a juxtaposition of the most conventional analysis methods.

3.2.3 Optimization of the TPD Setup

When performing TPD measurements one only wants to detect molecules desorbing from the front surface of the sample, later on referred to as species A, and not from the heating wires, the sides/backside of the crystal or from the incandescent manipulator (species B). With a conventional mass spectrometer setup without a Feulner cup, the partial pressures of A and B in the mass spectrometer and in the chamber are identical and determined by the desorption rate from the sample and the pumping speed of the vacuum pumps. To minimize the unwanted contributions from B to the mass spectrometer signal, a copper Feulner cup, depicted in Figure 8, was installed [92].

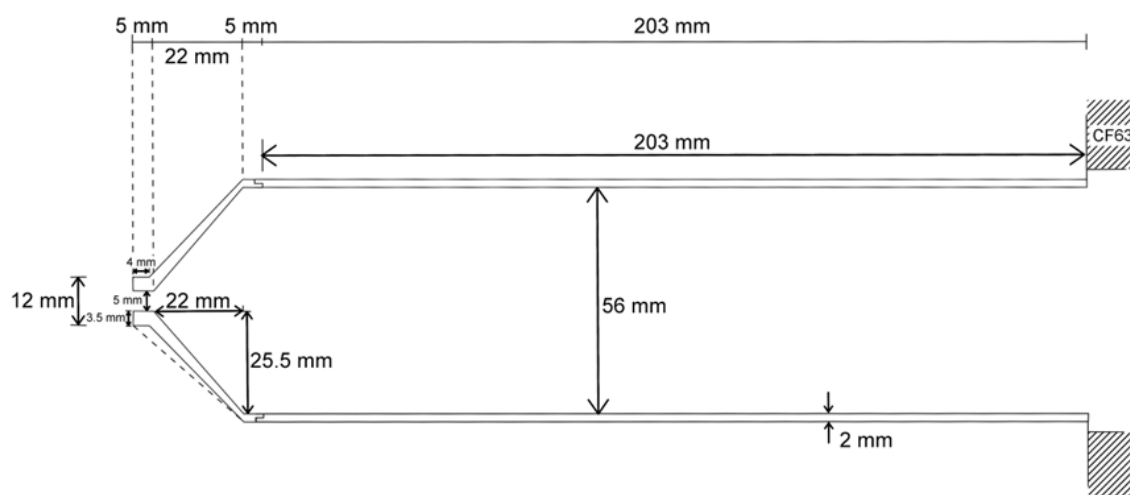


Figure 8: Drawing of the used Feulner cup.

The Feulner cup is a tube around the mass spectrometer with a small aperture (5 mm), which was approached within 1 mm to the sample surface, as shown in Figure 9. Differential pumping of the Feulner cup was possible through a valve to the analysis chamber, but the valve was kept closed to maximize the otherwise very small intensities from desorbing hydrogen. This meant that the pumping speed of the Feulner cup was determined by the flux

3. Experimental Methods

of molecules through the 5 mm opening facing to the sample, which can be assumed to be proportional to the flux through the opening had the sample not been there:

$$I = \frac{p}{\sqrt{2\pi mk_B T}}$$

with I the flux of the molecules had the sample not been there, p the partial gas pressure, m the mass of the molecules, k_B the Boltzmann's constant and T the temperature. Without the differential pumping by the analysis chamber, the Feulner cup has no effect on the partial pressure of B. The pressure of B inside the Feulner cup will be the same as the pressure of B outside the Feulner cup in the rest of the chamber. However, because the pressure of A inside the Feulner cup is determined by the pumping speed of the cup, which is much smaller than the pumping speed of the chamber, the pressure of A inside the cup becomes much larger than it would have been had the cup not been there. As a consequence the sensitivity to A becomes much larger than the sensitivity to B, and unwanted signals can, thus, be avoided.

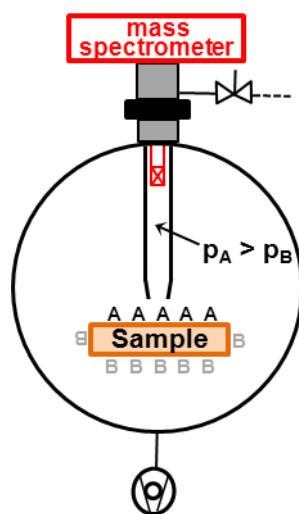


Figure 9: *The Feulner cup TPD setup.*

Because the pumping speed of the Feulner cup is determined by the opening facing the sample, the absolute pumping speed, and thereby the measured intensities, depends strongly on the distance between the Feulner cup and the sample. Comparing absolute intensities between two experiments is therefore only possible if the distance between Feulner cup and sample is identical. To achieve this, a mirror was installed to image the space between Feulner

cup and sample. However, the distance was adjusted by eye, and it would be a huge improvement if a scaled camera image could be used instead. To correct for this issue the integrated area for each TPD spectrum was normalized to the coverage of 2HTPP on the surface as measured by XPS.

Typical requirements for heating are a linear heating rate and that the linearity should be observable from the beginning to the end of the experiment. The settings at the temperature regulator (Eurotherm) should therefore always be re-adjusted when the sample mounting is changed. Usually, the heating rate is set between 0.1 - 10 K/s. For the measurements in this thesis, a relative high heating rate of 5 K/s was used to ensure a high partial pressure increase in the mass spectrometer relative to the background pressure of hydrogen always present in the chamber.

3.3 Ultra-High Vacuum Apparatus and Sample Preparation

In Figure 10, a picture of the ultra-high vacuum (UHV) chamber system is given. But why did we use UHV-conditions? In order to characterize a surface, the surface has to stay free of contamination during the experiment. The most time consuming experiments in this thesis were the investigation of the N 1s region of submonolayers of 2HTPP, which lasted up to four hours. During an experiment the sample surface is continuously struck by gas phase molecules. At a pressure p the incoming flux of gas molecules can be calculated as:

$$I = \frac{p}{\sqrt{2\pi m T k_B}}$$

m is the mass of the molecules, k_B is Boltzman's constant and T the absolute temperature. The vacuum chamber used in this thesis had a base pressure in the low 10^{-10} mbar regime, with the main components being hydrogen, water, CO and CO₂. Fortunately, these molecules do not adsorb on Cu(111) or Ag(100) at room temperature, but at low temperature especially adsorption of water can be a problem. Using the above equation, we can calculate how much water we would expect to adsorb on the sample surface during a four hour measurement at 100 K. We end up with ~ 30 ML, which well illustrates the importance of very good vacuum. A further reason for working in vacuum is that both XPS and TPD requires high vacuum. In XPS the emitted photoelectrons have to reach and travel through the analyzer without colliding with gas molecules. Similarly, in a mass spectrometer the ions created also have to

3. Experimental Methods

travel through the quadrupole without collisions. The mean free path, i.e. the average distance travelled before a collision happens, should be much larger than the distance the electrons and ions have to travel before reaching the respective detectors. At base pressures below 10^{-5} mbar this requirement is fulfilled, as the mean free path here exceeds 5 m.

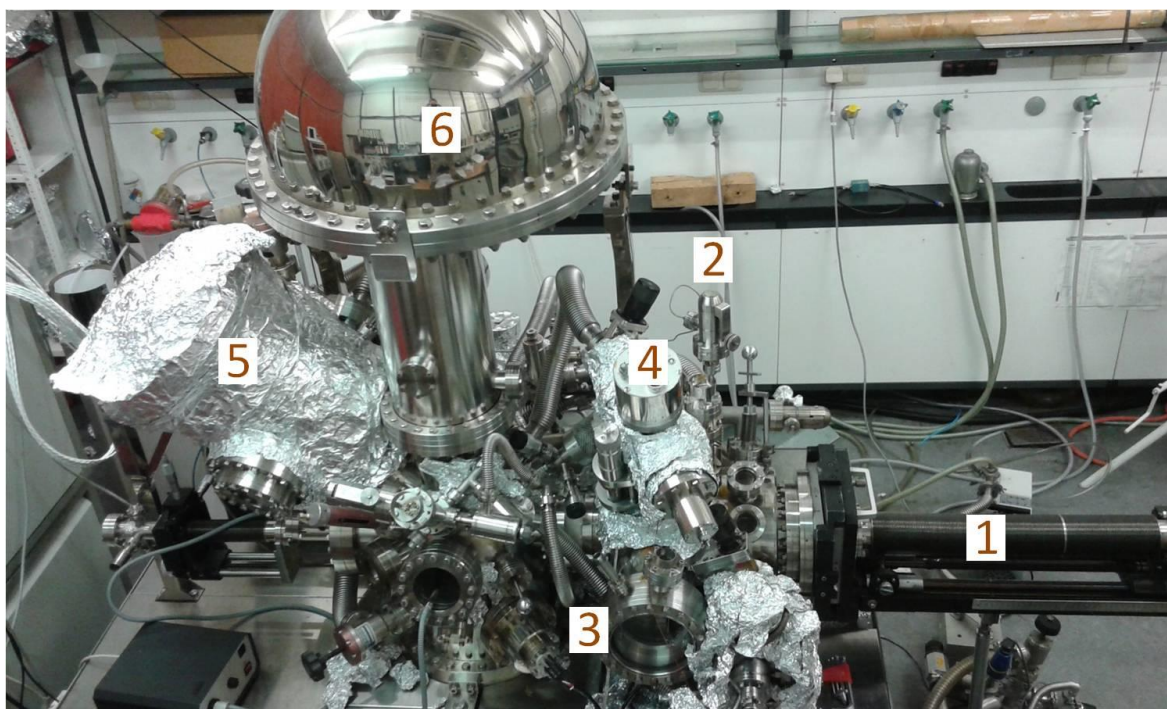


Figure 10: The *Scienta* ultrahigh vacuum chamber: manipulator arm (1), sputter gun (2), Knudsen cell (3), mass spectrometer (4), monochromator (5), SES 200 analyzer (6).

In the preparation chamber, visible on the right part of Figure 10, the following procedures were conducted:

Cleaning of the sample: The sample was sputtered with Ar^+ -ions (sputter gun (2)). The Ar pressure in the chamber was $5 \cdot 10^{-6}$ mbar and the ion energy 0.8 kV for the Ag(100) crystal and 1.0 kV for the Cu(111) crystal. In both cases, the sample current was 3-4 μA . By applying high voltage, Ar^+ -ions get accelerated and were literally shot at the surface. Through collisions with atoms in the surface, the impinging ions remove the topmost surface layers and a rough surface is left over. In order to recreate a flat and well-defined surface with wide terraces and a low amount of defects, the sample was heated for 15 minutes to 700 K for Ag(100) and 1000 K for Cu(111). This increases the mobility of the atoms in the surface and allows them to reorganize and minimize the surface energy.

3. Experimental Methods

Deposition of organic molecules on the surface was achieved by the use of a home-built Knudsen cell evaporator (3). The Knudsen cell consists of a quartz crucible surrounded by tantalum heating wires. The thermocouples are attached to the outside of the crucible. The radiative heating is enough to reach 580-640 K, the evaporation temperature of the porphyrins. Usually a closed-packed porphyrin layer was evaporated in 3-4 minutes.

Iron deposition was accomplished from a 1 mm in diameter iron rod with a purity of 99 % via an EFM 3 e-beam evaporator, where electrons from a hot filament were accelerated towards the iron rod with 800 V. The impinging high energy electrons then heat the rod. The emission current was 50 mA, resulting in a deposition rate of 0.05 ML/minute. Please note, that if you want to use a crucible for evaporation, possible reactions of the evaporant with the crucible must be considered [93].

TPD measurements were also performed in the preparation chamber (for further information: see Chapter 2.2).

In the second chamber, the analysis chamber, only the **XPS measurements** were performed. The photon source was an Al-K $_{\alpha}$ anode (1486.6 eV). The emitted light then passed a quartz-crystal monochromator (5). Depending on the lattice constant of the diffraction crystals and the given angle (θ), only light with a certain wave length interferes constructively due to Bragg reflection ($n\lambda = 2d\sin(\theta)$). Thereby, the natural line width (ΔE_{X-ray}) of the X-ray source is reduced from 0.85 eV to 0.2 eV, enhancing the overall energy resolution of the spectrometer (0.3 eV). However, by passing the monochromator, the intensity of the light is lowered. To enhance the intensity (= focusing the light), the anode, the diffraction crystals and the sample are arranged on Rowland Circles [94].

For electron detection, a scienta SES200 **hemispherical energy analyzer** (6) was used. The emitted photoelectrons have to pass an electrostatic lens system, which focuses the electrons towards the entrance slit, where the electrons are decelerated to the desired pass energy. The electric field between the inner and outer hemisphere is chosen such that only electrons with a certain energy $E_0 = |e|V_0$ are deflected in the correct arc to reach the analyzer. Reducing the pass energy leads to a better energy resolution, but lower intensities. The hemispherical analyzer was calibrated to the Fermi edge of gold ($E_B = 0$ eV) and the position of the Au 4f $_{7/2}$ peak, a XP feature with high intensity and small energetic width ($E_B = 83.8$ eV) [97].

4. Results

The following chapter gives an overview of the results on the metalation and dehydrogenation of tetrapyrroles on Cu(111) and Ag(100).

4.1 Tetrapyrroles on Cu(111)

4.1.1. Coverage- and Temperature-Dependent Metalation and Dehydrogenation of 2HTPP on Cu(111) [P1, P2]

The articles [P1] and [P2] are collaborations with the group of PD Dr. Hubertus Marbach (H. Marbach, Dr. S. Ditze, M. Stark) from the University Erlangen-Nürnberg, who measured and analyzed the STM images.

In previous studies it was reported that 2HTPP on Cu(111) can self-metalate with copper atoms from the underlying substrate [50, 52, 63, 108]. The aim of the current investigation was to demonstrate the influence of coverage on the rate of self-metalation. As illustrated in Figure 2, metalation is easily followed in XPS by following the conversion of the two non-equivalent nitrogen species of 2HTPP, i.e. aminic (400.05 eV, -NH-) and iminic (398.55 eV, =N-) nitrogen, into the single nitrogen species of the CuTPP. Following the metalation rate in STM, however, has to rely on the very different mobilities of 2HTPP and CuTPP on the surface. At low coverage, 2HTPP adsorbs at 300 K as individual molecules, orientated along one of the three high symmetry axes of the (111) crystal plane, and, due to the strong interaction of the iminic nitrogen atoms with the underlying copper substrate, the molecules are immobile and easy to image in STM [31, 32, 38, 40]. CuTPP, however, has a much weaker interaction between the iminic nitrogen atoms and the substrate and is therefore much more mobile on the surface than 2HTPP. As a result, CuTPP diffuses too fast at room temperature to be imaged in STM. At higher coverages, CuTPP islands are formed, but they coexist with the fast diffusing 2D gas phase. The rate of metalation in STM was, therefore, not measured by counting the metalated molecules, but instead by counting the remaining 2HTPP molecules on the surface after the reaction.

4. Results

Figure 11 shows representative STM images and XPS spectra used to measure the coverage-dependent rate of metalation presented in Figure 12. From Figure 12, it is immediately apparent that there is an abrupt increase in the rate of metalation as the coverage on the surface is increased beyond $0.36 \text{ molecules/nm}^2$. Assuming a first order reaction behavior, the rate of metalation can be calculated to increase by a factor of 20 between 0.36 and $0.54 \text{ molecules/nm}^2$. It is also apparent that there is a very high consistency between the STM and XPS data, despite the data being acquired on different machines and different crystals.

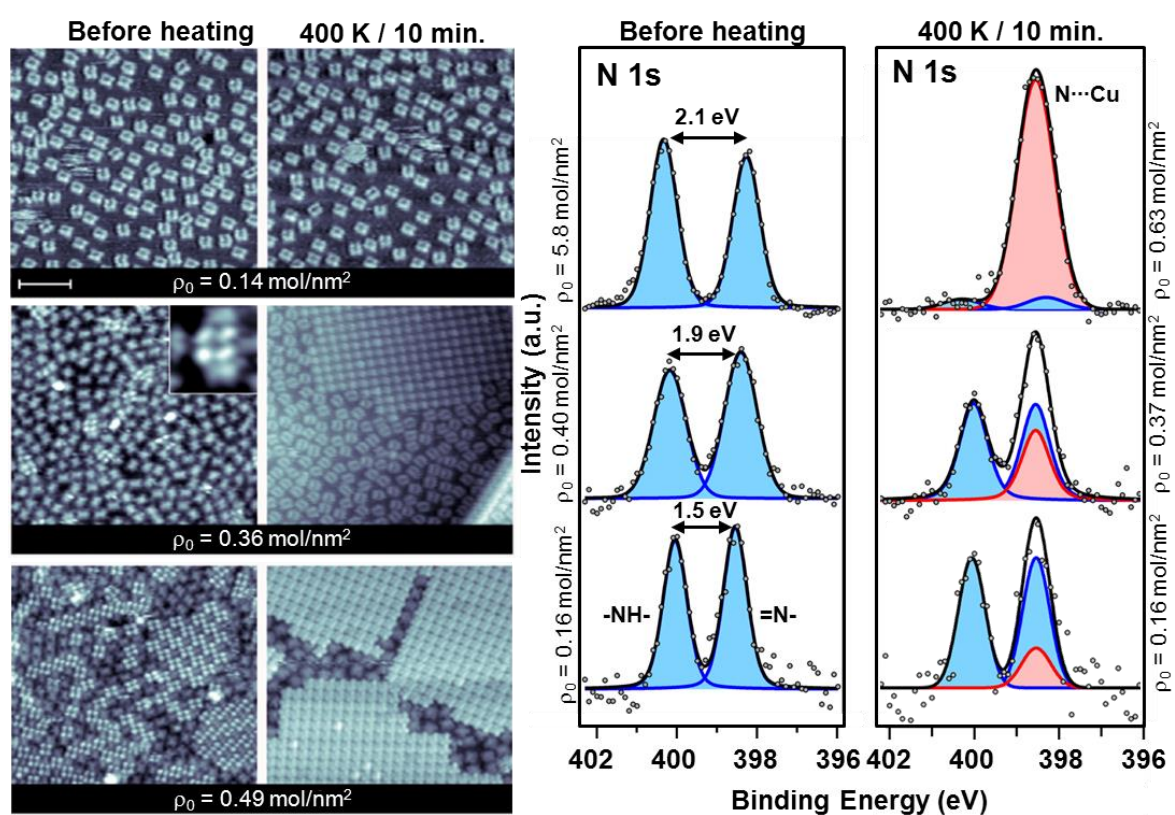


Figure 11: STM images (left) and XPS spectra (right) for different 2HTPP coverages on Cu(111) before and after heating to 400 K for 10 minutes.

The reason for the abrupt increase in the rate of metalation can be found in the STM images in Figure 11. As the coverage is increased above $0.36 \text{ molecules/nm}^2$, a checkerboard-like adsorption structure starts forming where every second molecule is elevated slightly above the surface [34]. At $0.54 \text{ molecules/nm}^2$, the checkerboard structure is completed, and multilayers start forming [34]. From the XPS data in Figure 11, the separation between the aminic and iminic N 1s peaks can be seen to increase as the checkerboard structure is formed, and it is

4. Results

possible to describe the checkerboard structure as an even combination of two types of molecules: molecules in direct contact with the surface, with a strong interaction between the iminic nitrogen atoms and the surface, and molecules slightly elevated above the surface, with a much weaker interaction between the iminic nitrogen atoms and the surface.

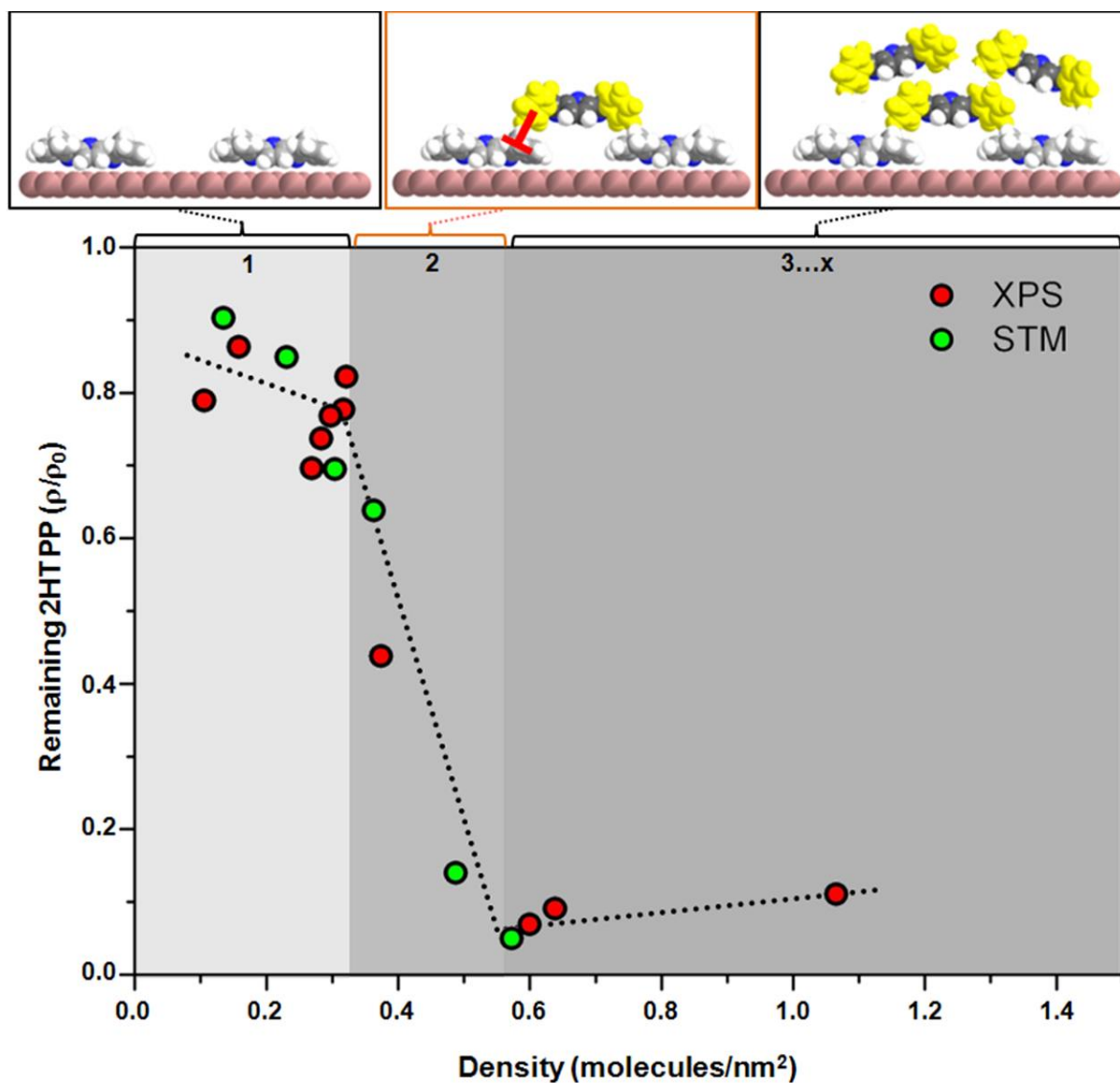


Figure 12: Coverage-dependent metalation of 2HTPP on Cu(111). The red (XPS) and green (STM) dots indicate the remaining 2HTPP molecules after heating to 400 K for 2 minutes. At low coverage metalation is slow, but increasing the coverage above 0.36 molecules/nm² abruptly increases of the rate of metalation.

In the transition state for the gas phase metalation reaction, the metal atom is coordinated to all four nitrogen atoms of the molecule. If the transition state for the surface reaction is similar, the interaction between the iminic nitrogen atoms and the surface will be broken in the transition state and a stronger or weaker bond between the iminic nitrogen atoms and the surface will shift the energy of the 2HTPP molecule relative to the transition state, as illustrated in Figure 13. The weaker nitrogen surface bond for the elevated molecules would therefore result in an increased rate of metalation, as observed.

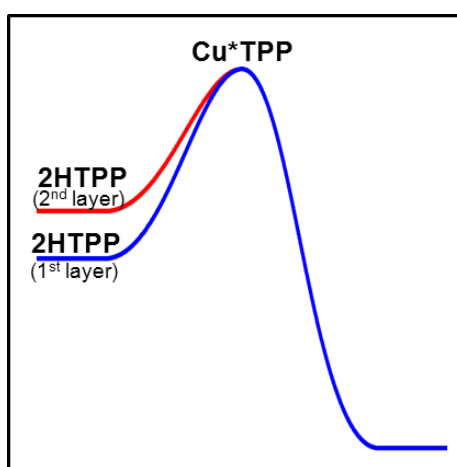


Figure 13: Possible reaction profile for 2HTPP self-metalation on Cu(111). 2HTPP molecules in direct contact with the surface are more stable compared to the molecule in the elevated layer of the checkerboard structure.

To support the above presented model, XPS measurements with very good statistics (long measuring times) were performed for 2HTPP at coverages of 0.24, 0.55, and 9.1 molecules/nm². These coverages correspond to a low coverage layer (low metalation rate), the full checkerboard structure (high metalation rate), and a multilayer. The spectra are shown in Figure 14, along with the corresponding fits. For the 2HTPP multilayer the typical peak separation of 2.03 eV (full width at half maximum (FWHM) = 0.83 eV) is observed, with shake-up satellites at ~2.9 eV higher binding energy. The smaller peak separation of only 1.50 eV (FWHM = 0.77 eV) for 0.24 molecules/nm² reflects the chemical interaction of the iminic nitrogen atoms with the substrate (see above). The checkerboard structure, i.e. 0.55 molecules/nm², is fitted with two doublets: one for the lower sublayer and one for the upper sublayer, yielding peak separations of 1.39 and 1.93 eV (all FWHM = 0.81eV), respectively.

4. Results

Within the error bars (± 0.05) these values are very similar to those of the lower sublayer and the multilayer, respectively. The unchanged (or even smaller) peak separation for the lower sublayer component in the checkerboard structure is a clear indication that lower sublayer molecules are bound as strong or stronger than the low coverage molecules; thus, a faster metalation rate of the lower sublayer molecules is ruled out, and we conclude that the dramatic increase of the metalation rate in the checkerboard structure is due to the metalation of the nearly undistorted molecules in the upper sublayer.

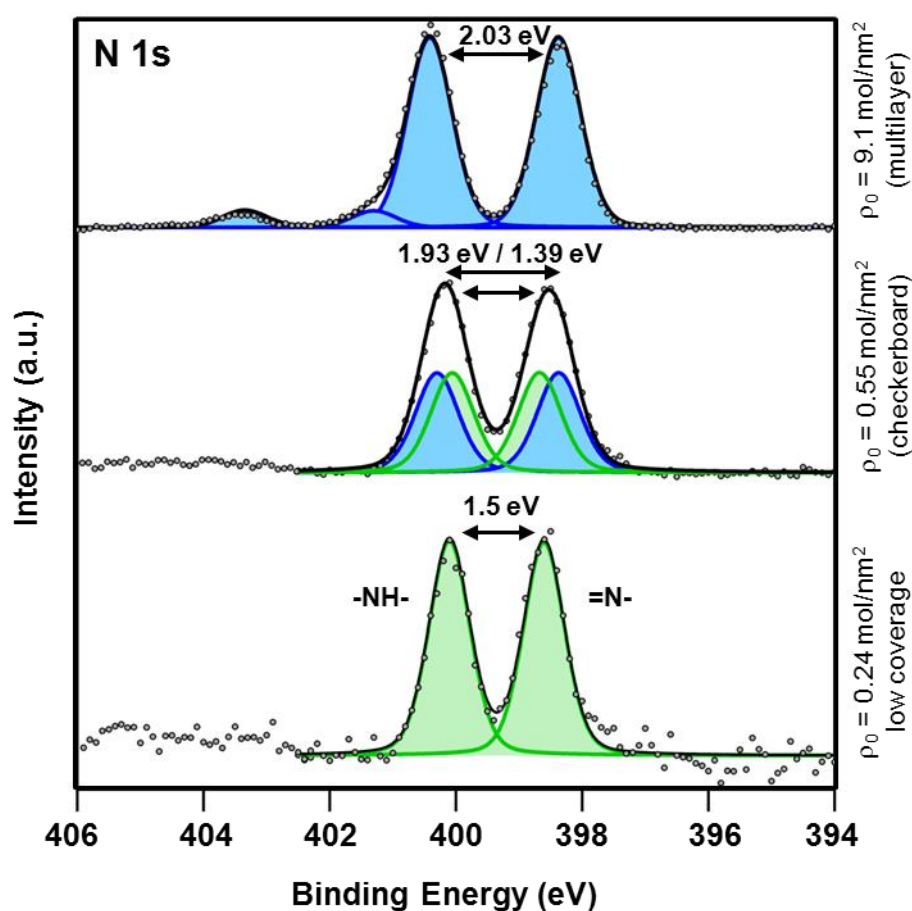


Figure 14: *N 1s* XPS spectra of 2HTPP on Cu(111) for 0.24, 0.55, 9.1 molecules/nm², corresponding to a low coverage layer (low metalation rate), the saturated checkerboard structure (high metalation rate) and a multilayer.

Not just metalation, but also dehydrogenation of 2HTPP on Cu(111) was investigated. The TPD spectra, depicted in Figure 15, give an overview of the coverage- and temperature-dependent reactions of the free-base porphyrin on Cu(111) from 280 to 1000 K. At a coverage of 0.56 molecules/nm², where the checkerboard structure is complete [34], three hydrogen

desorption peaks are visible. The first peak at 450 K was quickly confirmed to be metalation, since XPS after heating with 5 K/s to 490 K and immediately cooling back down to room temperature revealed full metalation.

The reaction at 550 K, producing the second TPD peak, could be identified from previous STM investigations by Ditze and Xiao *et al.* [51, 52] that revealed that CuTPP after metalation undergoes a two-step reaction, where first one side and then the other side of the molecule loses apparent height, resulting in a square shaped molecule. A similar observation, but with NEXAFS, was made by Di Santo *et al.* for 2HTPP on Ag(111). At 550 K, they observed that the phenyl rings of the 2HTPP molecule would rotate and become in plane with the rest of the molecule. Based on these findings, they suggested a partial dehydrogenation of the molecule, where adjacent phenyl and pyrrole rings fused together, resulting in a square molecule [95]. If the fusion of the phenyl and pyrrole rings were to happen first on one side of the molecule and then on the other side, as depicted in Figure 15, it would be consistent with the reaction observed by STM on Cu(111). A very similar reaction was also reported to occur in liquid medium [96].

The proposed fusion mechanism would involve the release of 4 hydrogen molecules, which agrees well with the integrated areas of the first two TPD peaks at 0.56 molecules/nm², which have a ratio of 1.0 : 3.8. Further heating to 1000 K leads to the release of 10.2 hydrogen molecules. Considering the total amount of 30 hydrogen atoms per porphyrin molecule the last step causes the complete dehydrogenation of the molecules.

At coverages below 0.30 molecules/nm², the two first TPD peaks are replaced by a single peak at 510 K. On the one hand XPS measurements after heating to 570 K at 5 K/s reveal full metalation and on the other hand STM measurements at this low coverage show the stepwise lowering of the molecule indicative of the fusion of the phenyl and pyrrole rings. Hence, the TPD peak at 510 K must be a combination of both reactions. The difference between low and high coverage spectra indicates that both reactions are strongly affected by coverage: at lower coverages metalation is slower and fusion of phenyl and pyrrole rings faster.

To understand the effect of coverage on the fusion of the phenyl and pyrrole rings, one has to consider the surface as it looks after metalation.

4. Results

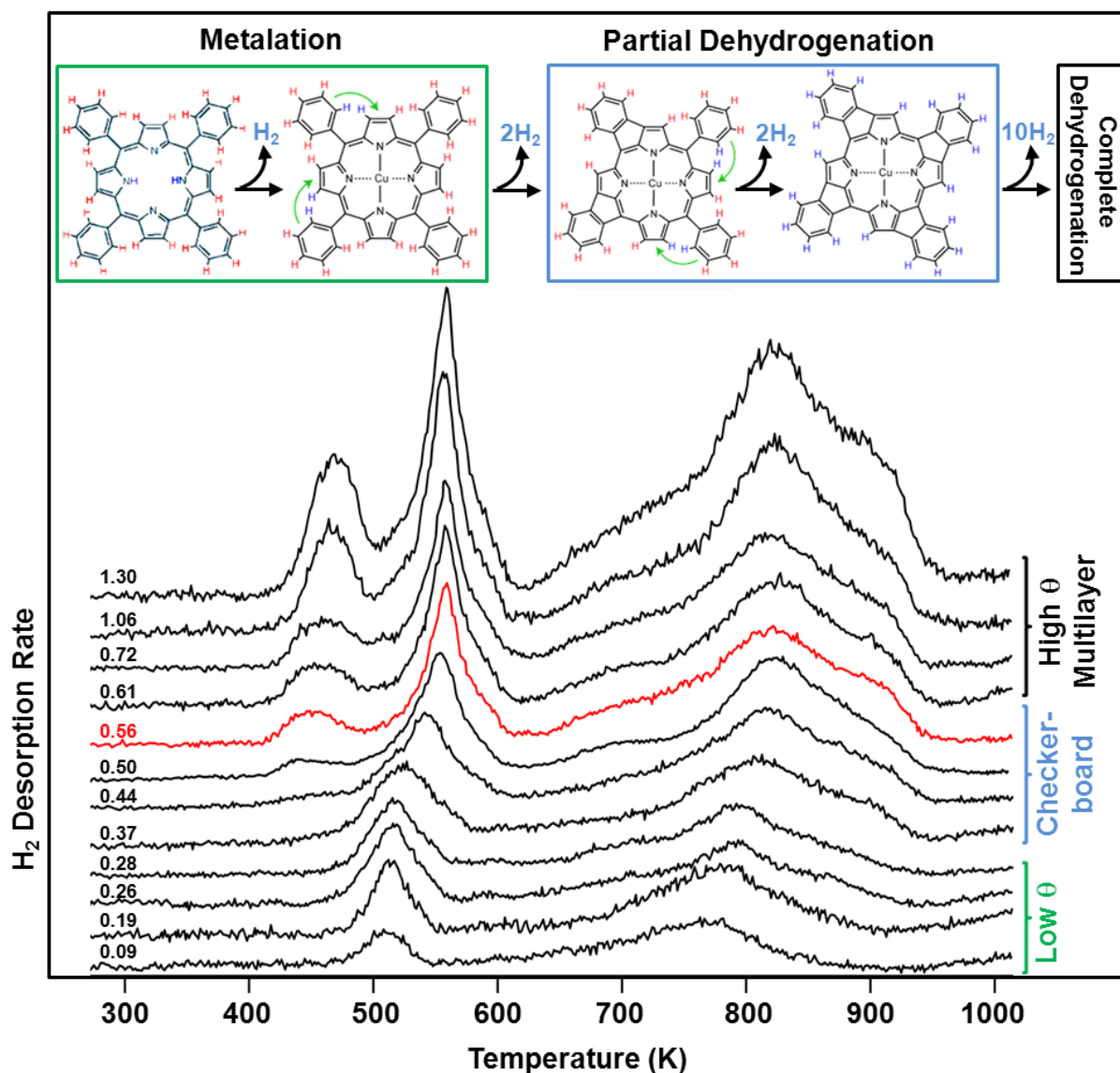


Figure 15: Coverage- and temperature dependent metalation and dehydrogenation of 2HTPP on Cu(111) with a heating rate of 5 K/s. The numbers next to the hydrogen desorption spectra indicate the initial coverage of 2HTPP in molecules/nm². The molecular models above show the metalation reaction and the suggested fusion of adjacent phenyl and pyrrole rings.

At low coverage, individual CuTPP molecules diffuse on the surface, while at high coverage CuTPP forms islands, stabilized by T-type interactions between phenyl rings of adjacent molecules [33, 50, 98]. As the fusion of phenyl and pyrrole rings requires the phenyl rings to rotate and become in plane with the molecule, the stabilizing T-type interactions in the islands represent an additional reaction energy barrier to overcome, and molecules in the islands, thus, react slower than freely diffusing CuTPP molecules.

4.1.2 Insights into the Self-Metalation Pathway of 2DTPP on Cu(111) [P3]

To be able to separate metalation and dehydrogenation in the TPD spectra in Figure 15, especially at low coverage, we decided to measure a few TPD spectra with a deuterated porphyrin molecule, tetraphenyl-21,23D-porphyrin (2DTPP), where the two central aminic hydrogen atoms had been replaced with deuterium. Metalation, releasing D_2 (mass 4), should now be easily distinguishable from dehydrogenation, releasing H_2 (mass 2). We were very fortunate to have Dominik Lungerich from the group of Prof. Dr. Norbert Jux from the organic chemistry department, who synthesized the deuterated molecule for us, while the groups of Prof. Dr. Jörg Libuda (A. Kaftan, M. Laurin, J. Libuda) and PD Dr. Hubertus Marbach (M. Stark, S. Ditze, H. Marbach) from the Chair of Physical Chemistry II of the University Erlangen-Nürnberg characterized the synthesized molecule by diffuse reflectance infrared Fourier transform spectroscopy (DRIFTS) [99] and mass spectrometry [77] measurements, respectively.

The characterization of the synthesized 2DTPP showed that only the aminic hydrogen atoms were replaced by deuterium, exactly what we wanted, but the degree of deuteration was not 100 %. Instead we had a mixture of 9 % 2HTPP, 45 % HDTPP and 46 % 2DTPP. One would, therefore, expect a metalation peak in TPD with exactly those ratios, while the fusion of phenyl and pyrrole rings and the complete dehydrogenation should release only H_2 .

The TPD spectra of 0.54 2DTPP molecules/nm² from Cu(111) is shown in Figure 16. The three principal reactions identified in Figure 15 are clearly separated, but the ratios of H_2 , HD and D_2 are not what we expected. Far less than expected HD and D_2 desorb during metalation, and a large amount of deuterium desorb as HD during fusion of the phenyl and pyrrole rings and complete dehydrogenation.

These observations cannot be explained by the reaction pathway suggested by DFT calculations for the gas phase reaction, where the two hydrogen atoms combine over the central metal atom and desorb as H_2 . The hydrogenated phenyl and pyrrole rings could subsequently dehydrogenate potentially releasing a hydrogen atom instead of the deuterium atom produced during metalation. This would enrich the periphery in deuterium, causing far less deuterium to desorb during metalation than expected and a large amount of deuterium to desorb during dehydrogenation of the periphery of the molecule, exactly as observed.

4. Results

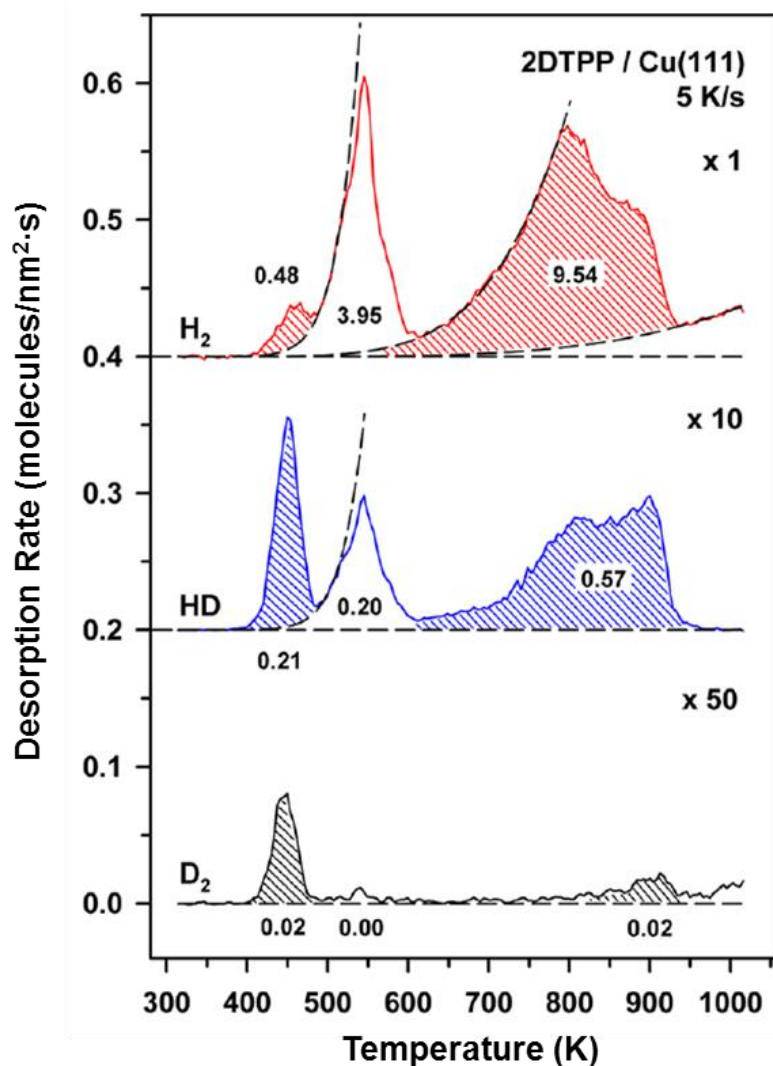


Figure 16: Desorption of mass 2 (H_2), mass 3 (HD) and mass 4 (D_2) from 0.54 2DTPP molecules/nm² on Cu(111) with a heating rate of 5 K/s. For clarity, HD and D_2 signals are magnified by factors of 10 and 50, respectively. The three reactions, metalation (450 K), partial dehydrogenation (545 K) and complete dehydrogenation (600 - 950 K) can be clearly identified. The numbers indicate the integrated areas, normalized to make the sum 15 (= 30 hydrogen atoms/2HTPP molecule).

This behavior can also explain another feature we observed. If we look closer at the position of the three TPD peaks for metalation, see Figure 17. It becomes apparent that D_2 desorbs slightly earlier than HD which desorbs slightly earlier than H_2 . As metalation starts the hydrogen and deuterium on the surface is produced almost exclusively from metalation and is therefore rich in deuterium. As the periphery of the molecule becomes more and more hydrogenated, the rate of dehydrogenation of the hydrogenated periphery increases, producing

more hydrogen and less deuterium on the surface, shifting the desorption from D₂ to HD and later H₂. Copper-based catalyst are known to catalyze both hydrogenation and dehydrogenation of hydrocarbons [100, 101], the reactions suggested are, therefore, not unusual for copper.

Figure 16 has a further interesting feature: when the desorption of H₂ and HD during complete dehydrogenation are compared, it becomes clear that the desorption maximum of HD is later than that of H₂. This can be explained as a kinetic isotope effect. The difference in ground state vibrational energy increases the activation energy barrier for dehydrogenation of a CD bond by 5 KJ/mol compared to a CH bond [102-105], thereby, shifting the desorption of HD to higher temperatures.

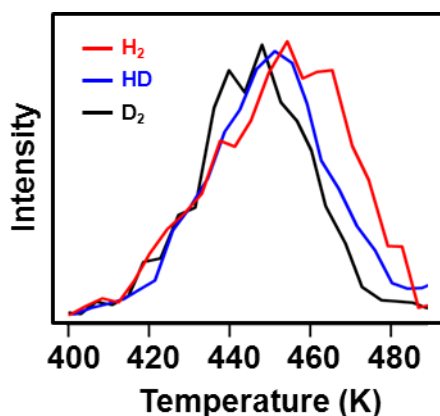


Figure 17: Normalized TPD peaks for the metalation of 0.54 molecules/nm² 2DTPP on Cu(111). The backgrounds caused by the fusion of phenyl and pyrrole rings, indicated by the dashed lines in Figure 13, have been subtracted.

Since metalation involves abstracting hydrogen atoms to the surface, the metalation of porphyrins, in general, might depend not only on the metal atom to be inserted, but also on the surface on which the reaction takes place; for typically used support materials such as oxides the stability of hydrogen could be very different from that on metal surfaces.

4.1.3 Metalation and Conformational Change of 2HTTBPP on Cu(111) [P4]

In a recent study by Ditze *et al.*, unique switching capabilities of 2H-tetrakis-(3,5-di-tert-butyl)-phenylporphyrin (2HTTBPP) on Cu(111) at room temperature were demonstrated [106]. The present investigation, article [P4] expands the understanding of the system by

4. Results

increasing the temperature up to 450 K. The group of PD Dr. Hubertus Marbach contributed the STM images, while I analyzed the XPS part.

The article concentrates on the self metalation with copper substrate atoms and the accompanying conformational change of 2HTTBPP on Cu(111). At room temperature, 2HTTBPP adsorbs in a bimodal structure, consisting of alternating rows of concave and convex molecules. Within this arrangement the individual molecules are able to switch between concave and convex conformations [106]. Slight heating to 330 K leads to an irreversible change to a monomodal structure, *hex A*. The molecules within the *hex A* structure have a similar appearance as the concave molecules in the bimodal conformation. Upon further heating to 350 K for 3.5 hours, partial metalation (57 %) of 2HTTBPP to CuTTBPP is observed in XPS. Heating further to 450 K for 2 minutes leads to full metalation and a change from the *hex A* to a *hex B* arrangement. In the *hex B* arrangement the apparent height of the center of the molecule has increased, as expected for a metalated molecule with a weaker molecule substrate interaction, see discussion in Section 4.1.1.

4.1.4 Metalation and Layer Exchange Mechanism of 2HPc on Cu(111) [P5]

The following research project, article [P5] was a collaboration with the group of Prof. Dr. J. Michael Gottfried (J. M. Gottfried, H.-J. Drescher, M. Chen). Within this study I measured most of the TPD spectra and also contributed to their analysis. The aim of the study was to give a more detailed description of the metalation process of free-base phthalocyanine (2HPc) multilayers on Cu(111). By XPS and TPD it could be proven that multilayers of 2HPc with a thickness of roughly 4 monolayer fully metalate at elevated temperatures (500 K). This raises the question of how the metalation of the multilayers occur: Are copper atoms diffusing into the 2HPc multilayers or do multilayer 2HPc molecules migrate to the copper surface and metalate there? To answer this question, multilayers of 2HPc were deposited on top of one monolayer of NiPc. Since monolayers had been shown not to desorb in TPD, no NiPc should desorb unless there is an exchange of molecules between mono- and multilayers. However, both CuPc and NiPc were observed desorbing, which can only be explained by the exchange of multilayer 2HPc molecules with monolayer NiPc molecules. 2HPc in direct contact with the surface immediately metalates and migrates back in the multilayer and desorbs from there. Although free copper atoms require a significant energy to produce (337 KJ/mol) [107], it

cannot be excluded that additional copper atoms diffuse in the multilayer and induce metalation there.

4.2 Metalation of Tetraphenylporphyrin with Iron on Ag(100) [P6]

In the next chapter, representing article [P6], I will present high-resolution XP data, showing the presence of a theoretically predicted Fe-2HTPP adcomplex as precursor for metalation. Metal-porphyrin adcomplexes as precursors for metalation have already been theoretically predicted for the gas phase reaction [48, 59, 65]. Also Kretschmann *et al.* reported about a possible intermediate state for the metalation of 2HTPP with Zn on Ag(111) [49]. To prove the existence of a precursor, a submonolayer coverage of 2HTPP was deposited on Ag(100) at 100 K. The resulting XP spectrum shows two peaks in the N 1s region, depicted in Figure 18, which can be attributed to iminic (=N-, 398.0 eV) and aminic (-NH-, 400.0 eV) nitrogen.

Upon adsorption of 0.12 ML iron at 100 K, which is 4-5 times the amount needed to fully metalate the adsorbed 2HTPP molecules, a 0.6 eV strong shift of the iminic N 1s peak can be observed, indicative of a direct interaction between the iminic nitrogen atoms and the deposited iron.

We expect that the Fe-2HTPP adcomplex for metalation is very similar to the theoretically predicted intermediate state by Shubina *et al.* [48], where Fe is equally bound to all four nitrogen atoms, while the aminic nitrogen atoms retain their bonding to the hydrogen atoms. On the right in Figure 18 a simplified illustration of the reaction is shown. Heating to 195 K for five minutes induces metalation, i.e. the formation of FeTPP. Further heating to 350 K leads to full metalation. In addition, high resolution data of the Fe 2p_{3/2} region was obtained, which was fitted according to Nefedov [69] and strongly resembles the appearance of FeTPP on Ag(111) and FePc on Au(111) [37,45,54, 69, 70].

4. Results

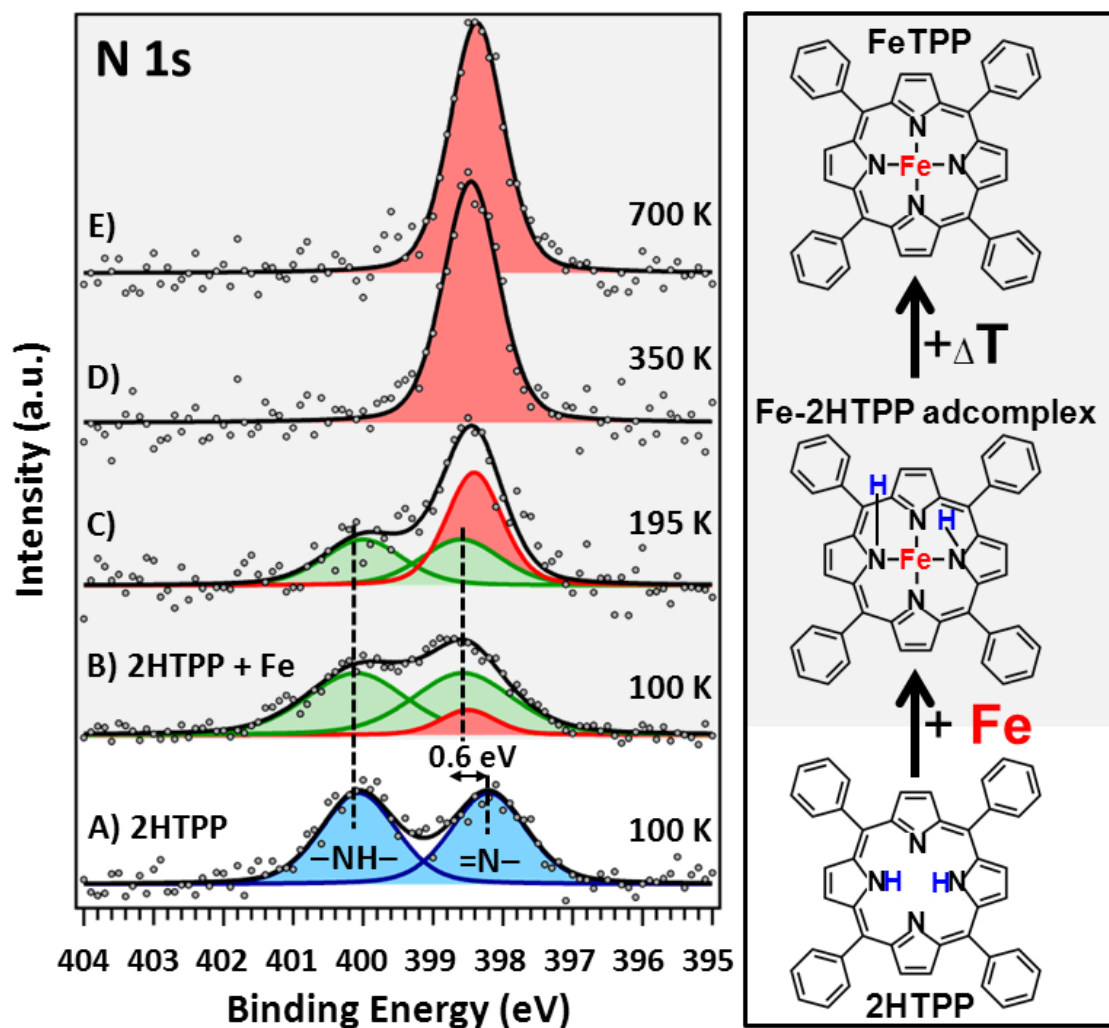


Figure 18: (left) $N1s$ spectra of 0.026 ML 2HTPP on Ag(100). A) Pure 2HTPP adsorbed on Ag(100) at 100 K shows two features, which can be attributed to aminic ($-NH-$, 400.0 eV) and iminic nitrogen ($=N-$, 398.0 eV). B) Upon iron deposition a shift of the iminic nitrogen of 0.6 eV towards higher binding energies is observed, which indicates the formation of a Fe-2HTPP adcomplex as precursor for metalation. C) Heating to 195 K initiates metalation, which D) is completed at 350 K. E) No further change is observed up heating to 700 K. (right) an illustration of the reactions.

5. Summary and Outlook

In the present combined X-ray photoelectron spectroscopy and temperature-programmed desorption study three tetrapyrroles (2HTPP, 2HPc and 2HTTBPP) on Cu(111) and Ag(100) were investigated. Within this research project it was possible to gain new insights in the metalation and dehydrogenation mechanisms and structural changes of these molecules at room temperature and above.

The first system investigated was **2HTPP on Cu(111)**. The focus was on metalation, dehydrogenation and the effect of coverage on the reactions. Upon heating, three different reactions could be identified: metalation of the center, fusion of adjacent phenyl and pyrrole rings and finally complete dehydrogenation of the porphyrin. Metalation and fusion of phenyl and pyrrole rings are both strongly coverage dependent. At low coverage, both reactions occur almost simultaneously, while coverages above 0.36 molecules/nm² leads to a formation of an elevated second layer, faster metalation and slower fusion of phenyl and pyrrole rings. The increased rate of metalation at higher coverages could be explained by a reduced interaction between the iminic nitrogen atoms and the surface, reducing the activation energy barrier for the reaction. The parallel decreased rate of fusion between phenyl and pyrrole rings could be explained by the formation of CuTPP islands stabilized by T-type interactions between adjacent molecules. Additional energy is required to rotate the phenyl rings in the islands and the reaction slows down.

By expanding the study to **2DTPP on Cu(111)** it was shown that the metalation does not proceed as suggested by gas phase DFT calculations, through the combination of the hydrogen atoms above the metal center, followed by desorption of H₂. The hydrogen atoms are instead transferred to the surface, opening two options: either direct recombination and desorption or scrambling with the periphery of the molecule. This leads to the conclusion that the surface is highly involved in the metalation process. The present study also showed that DFT calculation for the gas phase reaction cannot be simply transferred to surface reactions. To connect theory and experiment better, calculations that include the surface are needed. However, such calculations involving van der Waals interactions and very large molecules would be computationally very expensive.

5. Summary and Outlook

2HTTBPP on Cu(111) creates a bimodal structure at room temperature, wherein the molecules are able to switch between concave and convex conformations. Upon increasing the temperature to 330 K, the molecular arrangement irreversibly changes to a monomodal *hex* A conformation. The molecules within the *hex* A structure have a concave conformation, similar to the molecules in the bimodal structure. Further heating leads to metalation, i.e. the transformation of 2HTTBPP to CuTTBPP, and the formation of the *hex* B structure.

The metalation of submonolayer coverages of **2HPc on Cu(111)** already starts below 240 K. Heating to 450 K for 2 minutes leads to full metalation. Deposition of multilayers of 2HPc on top of a monolayer of NiPc on Cu(111), leads to intermixing and desorption of both CuPc and NiPc. Since the monolayer does not desorb, a layer exchange mechanism must exist, where NiPc at the Cu(111) surface is replaced by 2HPc, which, once at the surface, metalates to CuPc.

A theoretically predicted Fe-2HTPP adcomplex was observed when iron was codeposited with **2HTPP on Ag(100)**. The complex could be observed as a 0.6 eV shift of the iminic nitrogen peak to higher binding energies, compared to pure 2HTPP on Ag(100).

The present studies, all focused on metal surfaces, have shown that the substrate has a stronger influence on the reactions, especially metalation, than we initially expected. On different substrates, the reactions could behave very differently. It would, therefore, be interesting to study these reactions on more complex surfaces, such as oxide surfaces, often used for applications. Preliminary studies on 2HTPP on MgO(100) did reveal a surprising finding, namely that MgO(100) is able to self metalate 2HTPP molecules at room temperature. DFT calculations by Bernd Meyer suggest the reaction to be an ion exchange, where the two aminic protons in 2HTPP are exchanged for an Mg^{2+} ion, producing MgTPP and $\text{Mg}(\text{OH})_2$.

6. Zusammenfassung und Ausblick

In der vorliegenden Arbeit wurden drei verschiedene Tetrapyrrole (2HTPP, 2HPc und 2HTTBPP) auf Cu(111) und Ag(100) mittels Röntgenphotoelektronenspektroskopie (XPS) und Thermischer Desorptionsspektroskopie (TDS) untersucht. In diesem Zusammenhang war es möglich, neue Einblicke sowohl über den Metallierungs- und Dehydrogenierungsmechanismus als auch über Strukturveränderungen dieser molekularen Bausteine zu gewinnen.

Das zuerst untersuchte System war **2HTPP auf Cu(111)**. Im Fokus der Untersuchung stand der Einfluss der Ausgangsbedeckung auf die Oberflächenreaktionen des 2HTPP in Abhängigkeit von der Temperatur. Bei der Zufuhr von Wärme konnten drei aufeinanderfolgende Reaktionen identifiziert werden: Zuerst die Metallierung des Porphyrinzentrums, gefolgt vom Zusammenschluss benachbarter Phenyl- und Pyrrolringe und schließlich die komplette Dehydrogenierung des Porpyhrins. Die Metallierung und der Zusammenschluss benachbarter Phenyl- und Pyrrolringe sind stark von der Ausgangsbedeckung abhängig. Bei niedrigen Bedeckungen finden beide Reaktionen fast simultan statt. Bei Erhöhung der 2HTPP Bedeckung auf über $0.36 \text{ Molekülen/nm}^2$, wobei sich die Moleküle in einer Schachbrettstruktur anordnen, läuft die Metallierungsreaktion schneller und der Zusammenschluss der Phenyl- und Pyrrolringe langsamer ab. Die erhöhte Metallierungsrate bei höherer Bedeckung kann auf die geringere Wechselwirkung des iminischen Stickstoffs mit der Oberfläche zurückgeführt werden. Dies hat eine niedrigere Aktivierungsenergie der Metallierungsreaktion zur Folge. Gleichzeitig zeigt sich eine erniedrigte Zusammenschlussrate der Phenyl- und Pyrrolringe. Der Grund hierfür ist, dass sich CuTPP Moleküle vermehrt zu Inseln zusammenschließen, die über T-artige Wechselwirkungen zwischen benachbarten Phenylringen stabilisiert werden. Daher ist zusätzliche Energie notwendig um die Phenylringe des CuTPP Moleküls, das innerhalb der Insel angeordnet ist, zu drehen, was eine Verlangsamung der Reaktion zu Folge hat.

Bei der Untersuchung von **2DTPP auf Cu(111)** konnte gezeigt werden dass die Metallierungsreaktion, nicht wie die Gasphasenreaktion, durch die Kombination der Wasserstoffatome über dem Metallzentrum stattfindet, sondern, dass der Wasserstoff auf die

6. Zusammenfassung und Ausblick

Oberfläche über geht, auf der er: entweder sofort rekombiniert und desorbiert oder mit der Peripherie des Porphyrins reagiert, was zu einem Wasserstoff/Deuterium Austausch führt. Daraus kann gefolgert werden, dass die Oberfläche einen hohen Einfluss auf die Metallierungsreaktion hat. Die vorliegende Arbeit hat auch gezeigt, dass DFT Gasphasenberechnung nicht eins zu eins auf Oberflächenreaktion übertragen werden können. Um die Theorie und die experimentellen Erkenntnisse noch besser miteinander verknüpfen zu können, wären Berechnungen, die die Oberfläche mit berücksichtigen eine enorme Verbesserung. Jedoch sind Berechnungen, die die van der Waals Wechselwirkungen der Moleküle mit der Oberfläche und die sehr großen organischen Moleküle mit einschließen mit einem hohen Rechenaufwand verbunden.

2HTTBPP auf Cu(111) kann bei Raumtemperatur zwischen einer konkaven und einer konvexen intramolekularen Molekülgeometrie reversibel wechseln. Bei einer Temperaturerhöhung auf 330 K findet eine irreversible Transformation zur monomodalen *hex A* Konformation statt. Diese neue Struktur ähnelt der konkaven Konformation bevor dem Erwärmen. Weitere Wärmezufuhr führt zur Metallierung von 2HTTBPP zu CuTTBPP. Mit der Metallierung einhergehend findet eine weitere Strukturanpassung hin zur *hex B* Konformation statt.

Die Metallierung von weniger als einer Monolage **2HPc auf Cu(111)** findet ab 240 K statt, bei 450 K sind alle Moleküle zu CuPc metalliert. Das Abscheiden von 4 Moleküllagen 2HPc auf einer Monolage NiPc auf Cu(111) führt zum Austausch und gleichzeitigen Desorption von CuPc und NiPc. Da eine Monolage von CuPc oder NiPc auf Cu(111) nicht desorbiert, muss ein Austausch zwischen den einzelnen Lagen stattfinden, wobei NiPc im direkten Kontakt mit Cu(111) durch 2HPc Moleküle ersetzt werden. 2HPc Moleküle im direkten Kontakt mit der Kupferoberfläche werden dann zu CuPc metalliert.

2HTPP auf Ag(100) bildet einen theoretisch vorhergesagten Adkomplex mit gleichzeitig abgeschieden Eisen. Ein Indiz für diesen Komplex ist die Verschiebung des iminischen Stickstoffsignals um 0.6 eV hin zu höheren Bindungsenergien im Vergleich zu reinem 2HTPP auf Ag(100).

6. Zusammenfassung und Ausblick

Die gewonnenen Erkenntnisse dieser Arbeit beziehen sich ausschließlich auf Metallsubstrate. In dieser Untersuchung konnte gezeigt werden, dass das Substrat einen größeren Einfluss auf Oberflächenreaktionen, insbesondere auf die Metallierung großer organischer Moleküle, hat, als anfangs erwartet. Da die Reaktionen auf verschiedenen Substraten sehr unterschiedlich sein könnten, wäre ein nächster Schritt, das gewonnene Wissen auf komplexere Systeme zu übertragen, zum Beispiel oxidische Oberflächen, welche oft bei Anwendungen verwendet werden. Kürzlich haben Untersuchungen die Selbstmetallierung von 2HTPP auf MgO(100) bei Raumtemperatur gezeigt. DFT Berechnungen von Bernd Meyer schlagen einen Ionenaustausch vor, wobei die beiden Protonen des 2HTPP durch ein Mg^{2+} ersetzt werden und 2HTPP zu MgTPP reagiert und auf der Oberfläche $\text{Mg}(\text{OH})_2$ gebildet wird.

7. Acknowledgement

Finally it is a pleasure for me to acknowledge all the people who accompanied me during (at least) the last three years.

I want to greatly thank Prof Dr. Hans-Peter Steinrück. In 2009, you and PD Dr. Hubertus Marbach gave me the chance to experience the world of surface science during my Zulassungsarbeit. The excellent working conditions in the group both scientifically and inter-collegial inspired me to change my ways and start my research career. I have appreciated not only your excellent scientific expertise and our fruitful discussions, but also the help you have given me on the personal level.

Dr. Ole Lytken, I want to greatly thank you for all the support, helpful advise and great working atmosphere throughout my study. In particular, I appreciated the extensive scientific debates and your entrepreneurship, which never failed to improve things.

I also want to thank my closer colleagues, namely: Quratulain Tariq, Min Chen, Matthias Franke, Jie Xiao, Michael Stark, Stefanie Ditze, Sandra Krick-Calderon, Mathias Grabau, Daniel Wechsler and Martin Schmid. You always had a helping hand/advice for me, whenever I needed it and you significantly contributed to the very good working atmosphere. It was a pleasure to work with you.

I also want to thank all the collaborators, i.e. the group of PD. Dr. Hubertus Marbach (STM), the group of Prof. Dr. J. Michael Gottfried (TPD), the group of Prof. Dr Norbert Jux (synthesis of organic molecules) and the group of Prof. Dr. Jörg Libuda and the group of Dr. Mathias Laurin (molecules characterization with DRIFTS) for their great collaborations within the last three years.

In the field of surface science no one can do profound research without a strong team of technical experts. I, therefore, want to greatly thank Hans-Peter Bäumlner, Bernd Kreß, Friedhold Wölfel and the team of the mechanical workshop. Things always break from time to time, but you immediately solved the problems, fixed the devices or built new parts in very high quality and that within a short time.

I also want to thank all members at the Lehrstuhl für Phsikalische Chemie II for creating a great working atmosphere.

7. Acknowledgement

Besides my colleagues, I was strongly supported throughout by my family. I want to thank my parents, my sister and, especially, my wife, Giulia, for her patience, the time she spent on travelling to see me, and for her belief in us.

8. List of Figures

FIGURE	PAGE
Figure 1: <i>Space filling models of 2H-tetraphenylporphyrin (2HTPP), 2H-phthalocyanine (2HPc) and 2H-tetrakis-(3,5-di-tert-butyl)-phenylporphyrin (2HTTBPP).</i>	1
Figure 2: <i>As 0.41 molecules/nm² 2HTPP metalate on Cu(111), the two N 1s photoemission peaks, corresponding to the two nitrogen species of 2HTPP, aminic (=N-) at 398.55 eV and the iminic (-NH-) at 400.05 eV, merge into the single peak of CuTPP, where all four nitrogen atoms are equivalent.</i>	5
Figure 3: <i>Scheme of the energy profile of the gas phase metalation of 2HP with Co [48].</i>	6
Figure 4: <i>The Universal Curve, showing the inelastic mean free path as function of the kinetic energy of electrons [57].</i>	8
Figure 5: <i>XP spectrum of a clean Cu(111) surface, within the respective XP features are labeled.</i>	9
Figure 6: <i>Schematic illustration of a homogenous grown film A with a thickness x on a substrate B.</i>	11
Figure 7: <i>Hydrogen evolution from 0.72 2HTPP molecules/nm² on Cu(111).</i>	13
Figure 8 <i>Drawing of the used Feulner cup.</i>	15
Figure 9: <i>The Feulner cup TPD setup.</i>	16
Figure 10: <i>The Scienta ultrahigh vacuum chamber: manipulator arm (1), sputter gun (2), Knudsen cell (3), mass spectrometer (4), monochromator (5), SES 200 analyzer (6).</i>	18
Figure 11: <i>STM images (left) and XPS spectra (right) for different 2HTPP coverages on Cu(111) before and after heating to 400 K for 10 minutes.</i>	21
Figure 12: <i>Coverage-dependent metalation of 2HTPP on Cu(111). The red (XPS) and green (STM) dots indicate the remaining 2HTPP molecules after heating to 400 K for 2 minutes. At low coverage metalation is slow, but increasing the coverage above 0.36 molecules/nm² abruptly increases of the rate of metalation.</i>	22

8. List of Figures

FIGURE	PAGE
Figure 13: Possible reaction profile for 2HTPP self-metalation on Cu(111). 2HTPP molecules in direct contact with the surface are more stable compared to the molecule in the elevated layer of the checkerboard structure.	23
Figure 14: N 1s XP spectra of 2HTPP on Cu(111) for 0.24, 0.55, 9.1 molecules/nm ² , corresponding to a low coverage layer (low metalation rate), the saturated checkerboard structure (high metalation rate) and a multilayer.	24
Figure 15: Coverage- and temperature dependent metalation and dehydrogenation of 2HTPP on Cu(111) with a heating rate of 5 K/s. The numbers next to the hydrogen desorption spectra indicate the initial coverage of 2HTPP in molecules/nm ² . The molecular models above show the metalation reaction and the suggested fusion of adjacent phenyl and pyrrole rings.	26
Figure 16: Desorption of mass 2 (H ₂), mass 3 (HD) and mass 4 (D ₂) from 0.54 2DTPP molecules/nm ² on Cu(111) with a heating rate of 5 K/s. For clarity, HD and D ₂ signals are magnified by factors of 10 and 50, respectively. The three reactions, metalation (450 K), partial dehydrogenation (545 K) and complete dehydrogenation (600 - 950 K) can be clearly identified. The numbers indicate the integrated areas, normalized to make the sum 15 (= 30 hydrogen atoms/2HTPP molecule).	28
Figure 17: Normalized TPD peaks for the metalation of 0.54 molecules/nm ² 2DTPP on Cu(111). The backgrounds caused by the fusion of phenyl and pyrrole rings, indicated by the dashed lines in Figure 13, have been subtracted.	29
Figure 18: (left) N1s spectra of 0.026 ML 2HTPP on Ag(100). A) Pure 2HTPP adsorbed on Ag(100) at 100 K shows two features, which can be attributed to aminic (-NH-, 400.0 eV) and iminic nitrogen (=N-, 398.0 eV). B) Upon iron deposition a shift of the iminic nitrogen of 0.6 eV towards higher binding energies is observed, which indicates the formation of a Fe-2HTPP adcomplex as precursor for metalation. C) Heating to 195 K initiates metalation, which D) is completed at 350 K. E) No further change is observed up heating to 700 K. (right) an illustration of the reactions.	32

9. List of References

- [1] http://www.pm-magazin.de/zitate/michel-tournier_600622/ aufgerufen am **03.02.2015**.
- [2] D. S. Eisenberg, W. Kaunzmann *The structure and properties of water*, Oxford University Press, Oxford, **2005**.
- [3] J. N. Israelachvili, R. M. Pashley *Nature* **1983**, 306.
- [4] H. Malberg *Meteorologie und Klimatologie: Eine Einführung*, Springer, Berlin, **2006**.
- [5] J. H. Fuhrhop, K. M. Smith, in: *Porphyrins and Metalloporphyrins* (Ed.: K.M. Smith), Amsterdam, **1975**, pp. 757-869.
- [6] N.F. Phelan, M. Orchin *J. Chem. Educ.* **1968**, 45, 633-637.
- [7] N. Jux *Angew. Chem.* **2008**, 120, 2577–2581.
- [8] L. R. Migrom, *The Colours of Life. An Introduction to the Chemistry of Porphyrins and Related Compounds*, Oxford University Press, Oxford, **1997**.
- [9] K. S. Suslik, in: *The Porphyrin Handbook*, Vol. 4 (Eds.: K. M. Kadish, K. M. Smith, R. Guilard), Academic Press, San Diego, **2000**, pp. 41–60.
- [10] J. W. Buchler *Angew. Chem.* **1978**, 90, 425-441.
- [11] P. M. Tibbles, J. S. Edelsberg *Engl. J. Med.* **1996**, 334, 1642-1648.
- [12] G. M. Michael, A. Marroni, C. Longoni, in: *Handbook on Hyperbaric Medicine* (Eds.: G. Oriani, A. Marroni, F. Wattel), Springer, Berlin, **1996**, pp. 1-35.
- [13] S. R. Thom, R. L. Taber, I. Mendiguren, J. M. Clark, K. R. Hardy, A. B. Fisher *Ann. Emer. Med.* **1995**, 25, 474-480.
- [14] K. Seufert, M. L. Bocquet, W. Auwärter, A. Weber-Bargioni, J. Reichert, N. Lorente, J. V. Barth *Nature Chemistry* **2011**, 3, 114–119.
- [15] D. H. Lee, W. J. Lee, W. J. Lee, S. O. Kim, Y.-H. Kim *Phys. Rev. Lett.* **2011**, 106, 175502/1-4.
- [16] J. Knoll, S. Swavey *Inorganica Chimica Acta* **2009**, 362, 2989–2993.
- [17] S. Jiang, R. Cheng, X. Wang, T. Xue, Y. Liu, A. Nel, Y. Huang, X. F. Duan *Nat. Commun.* **2013**, 4, 2225/1-7.

9. List of References

- [18] B. R. Takulapalli, G. M. Laws, P. A. Liddell, J. Andreasson, Z. Erno, D. Gust, T. J. Thornton *J. Am. Chem. Soc.* **2008**, 130, 2226-2233.
- [19] A. H. Church *Philosophical Transactions of the Royal Society of London* **1869**, 627-636.
- [20] D. W. Bollivar, in: *The Porphyrin Handbook*, Vol. 13 (Eds.: K. M. Kadish, K. M. Smith, R. Guilard), Academic Press, San Diego, **2003**, pp. 49– 68.
- [21] A. Harrimann, J.-P. Sauvage *Chem. Soc. Rev.* **1996**, 25, 41-48.
- [22] V. A. Montes, C. Perez-Bolivar, N. Agarwal, J. Shinar, P. Anzenbacher Jr. *J. Am. Chem. Soc.* **2006**, 128, 12436-12438.
- [23] R. Paolesse, D. Monti, S. Nardis, C. Di Natale, in: *Handbook of Porphyrin Science Vol. 12* (Eds.: K. M. Kadish, K. M. Smith, R. Guilard), World Scientific, Singapore, **2011**, 121-225.
- [24] O. Fenwick, J. K. Sprafke, J. Binas, D. V. Kondratuk, F. Di Stasio, H. L. Anderson, F. Cacialli *Nano Lett.* **2011**, 11, 2451-2456.
- [25] E. M. Barea, V. Gonzalez-Pedro, T. Ripolles-Sanchis, H.-P. Wu, L.-L. Li, C.-Y. Yeh, E. W.-G. Diau, J. Bisquert *J. Phys. Chem C* **2011**, 115, 10898–10902.
- [26] C. W. Spangler *Proc. SPIE* **2008**, 6845, DOI: 10.1117/2.1200807.1228.
- [27] M. Erhirajan, Y. Chen, P. Joshi, R. K. Pandey *Chem. Soc. Rev.* **2011**, 340-362.
- [28] J.V. Barth *Surf. Sci.* **2009**, 603, 1533-1541.
- [29] I. Kröger, P. Bayersdorfer, B. Stadtmüller, C. Kleimann, G. Mercurio, F. Reinert, C. Kumpf *Phys. Rev. B* **2012**, 86, 195412/1-8.
- [30] H. Karacuban, M. Lange, J. Schaffert, O. Weingart, T. Wagner, R. Möller *Surf. Sci.* **2009**, 603, L39-L43.
- [31] G. Rojas, X. Chen, C. Bravo, J. H. Kim, J. S. Kim, J. Xiao, P. A. Dowben, Y. Gao, X. C. Zeng, W. Choe, A. Enders, *J. Phys. Chem. C* **2010**, 114, 9408-9415.
- [32] F. Buchner, E. Zillner, M. Röckert, S. Gläbel, H.-P. Steinrück, H. Marbach *Chem.-Eur. J.* **2011**, 17, 10226-10229.
- [33] G. Rojas, S. Simpson, X. M. Chen, D. A. Kunkel, J. Nitz, J. Xiao, P. A. Dowben, E. Zurek, A. Enders *Phys. Chem. Chem. Phys.* **2012**, 14, 4971-4976.
- [34] M. Stark, S. Ditze, M. Drost, F. Buchner, H.-P. Steinrück, H. Marbach *Langmuir* **2013**, 29, 4104-4110.

9. List of References

- [35] F. Buchner, K. G. Warnick, T. Wölfle, A. Görling, H.-P. Steinrück, W. Hieringer, H. Marbach *J. Phys. Chem. C* **2009**, 113, 16450-16457.
- [36] K. Comanici, F. Buchner, K. Flechtner, T. Lukasczyk, J. M. Gottfried, H.-P. Steinrück, H. Marbach *Langmuir* **2008**, 24, 1897-1901.
- [37] F. Buchner, K. Flechtner, Y. Bai, E. Zillner, I. Kellner, H.-P. Steinrück, H. Marbach, J. M. Gottfried *J. Phys. Chem. C* **2008**, 112, 15458-15465.
- [38] F. Buchner, J. Xiao, E. Zillner, M. Chen, M. Röckert, S. Ditze, M. Stark, H.-P. Steinrück, J. M. Gottfried, H. Marbach *J. Phys. Chem. C* **2011**, 115, 24172-24177.
- [39] H. Marbach, H.-P. Steinrück *Chem. Commun.* **2014**, 50, 9034-9048.
- [40] M. Eichberger, M. Marschall, J. Reichert, A. Weber-Bargioni, W. Auwärter, R. L. C. Wang, H. J. Kreuzer, Y. Pennec, A. Schiffrin, J. V. Barth *Nano Lett.* **2008**, 8, 4608-4613.
- [41] D. Écija, M. Trelka, C. Urban, P. de Mendoza, E. Mateo-Marti, C. Rogero, J. A. Martín-Gago, A. M. Echavarren, R. Otero, J. M. Gallego, R. Miranda *J. Phys. Chem. C* **2008**, 112, 8988-8994.
- [42] G. Di Santo, C. Castellarin-Cudia, M. Fanetti, B. Taleatu, P. Borghetti, L. Sangaletti, L. Floreano, E. Magnano, F. Bondino *J. Phys. Chem. C* **2011**, 115, 4155-4162.
- [43] G. Di Santo, C. Sfiligoj, C. Castellarin-Cudia, A. Verdini, A. Cossaro, A. Morgante, L. Floreano, A. Goldoni *Chem. - Eur. J.* **2012**, 18, 12619-12623.
- [44] A. Weber-Bargioni, J. Reichert, A. P. Seitsonen, W. Auwärter, A. Schiffrin, J. V. Barth *J. Phys. Chem. C* **2008**, 112, 3453-3455.
- [45] W. Hieringer, K. Flechtner, A. Kretschmann, K. Seufert, W. Auwärter, J. V. Barth, A. Görling, H.-P. Steinrück, J. M. Gottfried *J. Am. Chem. Soc.* **2011**, 133, 6206-6222.
- [46] M. Grobosch, V. Y. Aristov, O. V. Molodtsova, C. Schmidt, B. P. Doyle, S. Nannarone, M. Knupfer *J. Phys. Chem. C* **2009**, 113, 13219-13222.
- [47] K. Flechtner, A. Kretschmann, H.-P. Steinrück, J. M. Gottfried *J. Am. Chem. Soc.* **2007**, 129, 12110-12111.
- [48] T. E. Shubina, H. Marbach, K. Flechtner, A. Kretschmann, N. Jux, F. Buchner, H.-P. Steinrück, T. Clark, J. M. Gottfried *J. Am. Chem. Soc.* **2007**, 129, 9476-9483.
- [49] A. Kretschmann, M.-M. Walz, K. Flechtner, H.-P. Steinrück, J. M. Gottfried *Chem. Commun.* **2007**, 6, 568-570.
- [50] K. Diller, F. Klappenberger, M. Marschall, K. Hermann, A. Nefedov, Ch. Wöll, J. V. Barth *J. Chem. Phys.* **2012**, 136, 014705/1-13.

9. List of References

- [51] J. Xiao, S. Ditze, M. Chen, F. Buchner, M. Stark, M. Drost, H.-P. Steinrück, J. M. Gottfried, H. Marbach *J. Phys. Chem. C* **2012**, 116, 12275 – 12282.
- [52] S. Ditze, M. Stark, M. Drost, F. Buchner, H.-P. Steinrück, H. Marbach *Angew. Chem., Int. Ed.* **2012**, 51, 1–5.
- [53] W. Auwärter, D. Écija, F. Klappenberger, J. V. Barth *Nature Chemistry* **2015**, 7, 105-120.
- [54] Y. Bai, F. Buchner, M. T. Wendahl, I. Kellner, A. Bayer, H.-P. Steinrück, H. Marbach, J. M. Gottfried *J. Phys. Chem. C* **2008**, 112, 6087-6092.
- [55] T. Lukasczyk, K. Flechtner, L.R. Merte, N. Jux, F. Maier, J.M. Gottfried, H.-P. Steinrück *J. Phys. Chem. C* **2007**, 111, 3090-3098.
- [56] F. Buchner; V. Schwald, K. Comanici; H.-P. Steinrück; H. Marbach *ChemPhysChem* **2007**, 8, 241-243.
- [57] F. Buchner, K. Seufert, W. Auwärter, D. Heim, J. V. Barth, K. Flechtner, J. M. Gottfried, H.-P. Steinrück, H. Marbach *ACS Nano* **2009**, 3, 1789–1794.
- [58] J. M. Gottfried, H. Marbach *Z. Phys. Chem.* **2009**, 223, 53-74.
- [59] Y. Li, J. Xiao, T. E. Shubina, M. Chen, Z. Shi, M. Schmid, H.-P. Steinrück, J. M. Gottfried, N. Lin *J. Am. Chem. Soc.* **2012**, 134, 6401–6408.
- [60] F. Hanke, S. Haq, R. Raval, M. Persson *ACS Nano* **2011**, 5, 9093–9103.
- [61] J. Adisojoso, Y Li, J. Liu, P. N. Liu, N. Lin *J. Am. Chem. Soc.* **2012**, 134, 18526–18529.
- [62] C. M. Doyle, S. A. Krasnikov, N. N. Sergeeva, A. B. Preobrajenski, N. A. Vinogradov, Y. N. Sergeeva, M. O. Senge, A. A. Cafolla *Chem. Commun.* **2011**, 47, 12134–12136.
- [63] R. Gonzalez-Moreno, C. Sanchez-Sanchez, M. Trelka, R. Otero, A. Cossaro, A. Verdini, L. Floreano, M. Ruiz-Bermejo, A. Garcia-Lekue, J. A. Martin-Gago, C. Rogero *J. Phys. Chem. C* **2011**, 115, 6849–6854.
- [64] A. Sperl, J. Kröger, R. Berndt *Angew. Chem., Int. Ed.* **2011**, 50, 5294-5297.
- [65] T. E. Shubina *Adv. Inorg. Chem.* **2010**, 62, 261–299.
- [66] A. Einstein *Ann Physik* **1905**, 17, 132-148.
- [67] M. P. Seah and W. A. Dench *Surf Interface Anal.* **1979**, 1, 2-11.
- [68] R. P. Gupta, S. K. Sen *Phys. Rev. B* **1975**, 12, 15-19.

9. List of References

- [69] V. I. Nefedov *Izv. Nats. Akad. Nauk Resp., Ser. Fiz.* **1964**, 28, 816-822.
- [70] M. Schmid, J. Zirzmeier, H.-P. Steinrück, J. M. Gottfried *J. Phys. Chem. C* **2011**, 115, 17028-17035.
- [71] R. P. Gupta, S. K. Sen *Phys. Rev. B* **1974**, 10, 71-77.
- [72] S. Hüfner, in: *Photoelectron Spectroscopy* (Ed.: M. Cardona), Springer, Berlin, **1996**.
- [73] K. Oura, V. G. Lifshits, A. A. Saranin, A. V. Zotov, M. Karayama, in: *Surface Science: An Introduction*, Springer, Berlin, **2003**.
- [74] D. Wagner, L. E. Davis, M. V. Zeller, J. A. Taylor, R. H. Raymond, L. H. Gale *Surf. Interface Analy.* **1981**, 3, 211-225.
- [75] N. Stojilovic *J. Chem. Educ.* **2012**, 89, 1331–1332.
- [76] J. H. Scofield *J. Electron Spectrosc. Relat. Phenom.* **1976**, 8, 129-137.
- [77] Ed. de Hoffmann, V. Stroobant: *Mass Spectrometry: Principles and Applications*, Wiley-VCH Verlag GmbH, Weinheim, **2007**.
- [78] C.-M. Chan, R. Aris, W.H. Weinberg *Appl. Surf. Sci.* **1978**, 1, 360—376.
- [79] E. Habenschaden, J. Kippers *Surface Science* **1984**, 138, L147-L150.
- [80] J.M. Soler, N. Garcia *Surf. Sci.* **1983**, 124, 563-570.
- [81] A.M. de Jong, J.W. Niemantsverdriet *Surf. Sci.* **1990**, 233, 355-365.
- [82] D. L. S. Nieskens, A.P. van Bavel, J.W. Niemantsverdriet *Surf. Sci.* **2003**, 546, 159–169.
- [83] J. L. Falconer, J. A. Schwarz *Catal. Rev.-Sci. Eng.* **1983**, 25, 141-227.
- [84] D. A. King *Surf. Sci.* **1975**, 47, 384-402.
- [85] P. A. Redhead *Vacuum* **1962**, 12, 203-244.
- [86] A. J. Gellman, K. R. Paserba *J. Phys. Chem. B* **2002**, 106, 13231–13241.
- [87] C. T. Campbell, Y. K. Sun, W. H. Weinberg *Chem. Phys. Lett.* **1991**, 179, 53–57.
- [88] K. A. Fichthorn, R. A. Miron *Phys. Rev. Lett.* **2002**, 89, 96103/1-4.
- [89] S. L. Tait, Z. Dohnálek, C. T. Campbell, B. D. Kay *J. Chem Physics* **2005**, 122, 164708.

9. List of References

- [90] L. Mandeltort, D.-L. Chen, W. A. Saidi, J. K. Johnson, M. W. Cole, J. T. Yates Jr. *J. Am. Chem. Soc.* **2013**, 135, 7768–7776.
- [91] J. M. Gottfried, E. K. Vestergaard, P. Bera, C. T. Campbell *J. Phys. Chem. B* **2006**, 110, 17539-17545.
- [92] P. Feulner, D. J. Menzel *J. Vac. Sci. Technol.* **1980**, 17, 662-663.
- [93] K. J. Ross, B. Sonntag *Rev. Sci. Instrum.* **1995**, 66, 4409-4433.
- [94] P. Glatzel, M. Sikora, G. Smolentsev, M. Fernandez-Garcia *Catal. Today* **2009**, 145, 294–299.
- [95] G. Di Santo, S. Blankenburg, C. Castellarin-Cudia, M. Fanetti, P. Borghetti, L. Sangaletti, L. Floreano, A. Verdini, E. Magnano, F. Bondino *Chem. Eur. J.* **2011**, 17, 14354 – 14359.
- [96] D.-M. Shen, C. Liu, Q. Y. Chen *J. Org. Chem.* **2006**, 71, 6508 –6511.
- [97] H. D. Polaschegg *Appl. Phys.* **1974**, 4, 63-68.
- [98] J. Brede, M. Linares, S. Kuck, J. Schwöbel, A. Scarfato, S. H. Chang, G. Hoffmann, R. Wiesendanger, R. Lensen, P. H. J. Kouwer, J. Hoogboom, A. E. Rowan, M. Bröring, M. Funk, S. Stafström, F. Zerbetto, R. Lazzaroni *Nanotechnology* **2009**, 20, 275602/1-10.
- [99] M. B. Mitchell *Advances in Chemistry* **2009**, 236, 51–375.
- [100] J. Jenck, J.-E. Germain *J. Catal.* **1980**, 65, 141–149.
- [101] J. H. Sinfelt, J. L. Carter, D. J. C. Yates *J. Catal.* **1972**, 24, 283–296.
- [102] G. Soto, W. de La Cruz, H. M. J. Farias *J. Electron Spectrosc. Relat. Phenom.* **2004**, 135, 27–39.
- [103] P. R. Davies, N. Shukla *Surf. Sci.* **1995**, 322, 8 – 20.
- [104] F. Klappenberger, A. Weber-Bargioni, W. Auwärter, M. Marschall, A. Schiffrin, J. V. Barth *J. Chem. Phys.* **2008**, 129, 214702/1 –10.
- [105] Y.-P. Lin, O. Ourdjini, L. Giovanelli, S. Clair, T. Faury, Y. Ksari, J.-M. Themlin, L. Porte, M. J. Abel *J. Phys. Chem. C* **2013**, 117, 9895 –9902.
- [106] S. Ditze, M. Stark, F. Buchner, A. Aichert, N. Jux, N. Luckas, A. Görling, W. Hierarchy, J. Hornegger, H.-P. Steinrück, H. Marbach *J. Am. Chem. Soc.* **2014**, 136, 1609.
- [107] J. D. Cox, D. D. Wagman, V. A. Medvedev, V. A. Codata *Key Values for Thermodynamics*; Hemisphere Publishing Corp., New York, **1984**.

9. List of References

[108] S. Haq, F. Hanke, M. S. Dyer, M. Persson, P. Iavicoli, D. B. Amabilino, R. Raval *J. Am. Chem. Soc.* **2011**, 133, 12031 –12039.

[109] T. Ida, M. Ando H. Toraya *J. Appl. Cryst.* **2000**, 33, 1311-1316.

[110] D. M. Paese *Phys. Rev. B* **1991**, 44, 6708-6714.

[111] R. Hesse, P. Streubel, R. Szargan. *Surf. Interf. Anal.* **2007**, 39, 381-391.

10. Appendix [P1] – [P6]

[P1] [Abrupt Coverage-Induced Enhancement of the Self-Metalation of Tetraphenylporphyrin with Cu\(111\)](#)

Michael Röckert, Stefanie Ditze, Michael Stark, Jie Xiao, Hans-Peter Steinrück, Hubertus Marbach, Ole Lytken *J. Phys. Chem. C* **2014**, 118, 1661–1667.

[P2] [Coverage- and Temperature-Dependent Metalation and Dehydrogenation of Tetraphenylporphyrin on Cu\(111\)](#)

Michael Röckert, Matthias Franke, Quratulain Tariq, Stefanie Ditze, Michael Stark, Patrick Uffinger, Daniel Wechsler, Upendra Singh, Jie Xiao, Hubertus Marbach, Hans-Peter Steinrück, Ole Lytken *Chem. Eur. J.* **2014**, 20, 8948 – 8953.

[P3] [Insights in Reaction Mechanistics: Isotopic Exchange during the Metalation of Deuterated Tetraphenyl-21,23D-porphyrin on Cu\(111\)](#)

Michael Röckert, Matthias Franke, Quratulain Tariq, Dominik Lungerich, Norbert Jux, Michael Stark, Andre Kaftan, Stefanie Ditze, Hubertus Marbach, Mathias Laurin, Jörg Libuda, Hans-Peter Steinrück, Ole Lytken *J. Phys. Chem. C* **2014**, 118, 26729–26736.

[P4] [Massive conformational changes during thermally induced self-metalation of 2H-tetrakis-\(3,5-di-tert-butyl\)-phenylporphyrin on Cu\(111\)](#)

Michael Stark, Stefanie Ditze, Michael Lepper, Liang Zhang, Hannah Schlott, Florian Buchner, Michael Röckert, Min Chen, Ole Lytken, Hans-Peter Steinrück, Hubertus Marbach *Chem. Commun.* **2014**, 50, 10225-10228.

[P5] [Coordination Reactions and Layer Exchange Processes at a Buried Metal–Organic Interface](#)

Min Chen, Michael Röckert, Jie Xiao, Hans-Jörg Drescher, Hans-Peter Steinrück, Ole Lytken, J. Michael Gottfried *J. Phys. Chem. C* **2014**, 118, 8501–8507.

[P6] [Evidence for a Precursor Adcomplex During the Metalation of 2HTPP with Iron on Ag\(100\)](#)

Michael Röckert, Matthias Franke, Quratulain Tariq, Hans-Peter Steinrück, Ole Lytken *Chem. Phys. Lett.* **2015**, 635, 60-62.